Biological and Genetic Determinants of Glycolysis: Phosphofructokinase Isoforms Boost Energy Status of Stored Red Blood Cells and Transfusion Outcomes

Travis Nemkov,[1,2] Daniel Stephenson,[1] Eric J. Earley,[3] Gregory R Keele,[4] Ariel Hay,[5] Alicia Key,[1] Zachary Haiman,[6] Christopher Erickson,[1] Monika Dzieciatkowska,[1] Julie A. Reisz,[1] Amy Moore,[3] Mars Stone,[7,8] Xutao Deng, [7,8] Steven Kleinman,[9] Steven L Spitalnik,[10] Eldad A Hod,[10] Krystalyn E Hudson,[10] Kirk C Hansen,[1,2] Bernhard O. Palsson,[6] Gary A Churchill,[4] Nareg Roubinian, [7,8,11] Philip J. Norris, [7,8] Michael P. Busch, [7,8] James C Zimring,[5] Grier P. Page,[3] Angelo D'Alessandro[1,2*]

1) Department of Biochemistry and Molecular Genetics, University of Colorado Denver – Anschutz Medical Campus, Aurora, CO, USA;
2) Omix Technologies Inc, Aurora, CO, USA;
3) RTI International, Atlanta, GA, USA;
4) Jackson lab, Bar Harbor, ME, USA;
5) Department of Pathology, University of Virginia, Charlottesville, VA, USA;
6) Department of Bioengineering, University of California San Diego, La Jolla, CA, USA;
7) Vitalant Research Institute, San Francisco CA, USA;
8) Department of Laboratory Medicine, University of California San Francisco, CA, USA
9) University of British Columbia, Victoria, British Columbia, Canada;
10) Department of Pathology, Columbia University Irving Medical Center, New York, NY, USA;
11) Kaiser Permanente Northern California Division of Research, Oakland, CA

***Corresponding author:**

Angelo D'Alessandro, PhD
Department of Biochemistry and Molecular Genetics
University of Colorado Anschutz Medical Campus
12801 East 17th Ave., Aurora, CO 80045
Phone # 303-724-0096
E-mail: angelo.dalessandro@cuanschutz.edu

Running title: *Biological and Genetic Determinants of Red Blood Cell Glycolysis*

Graphical abstract

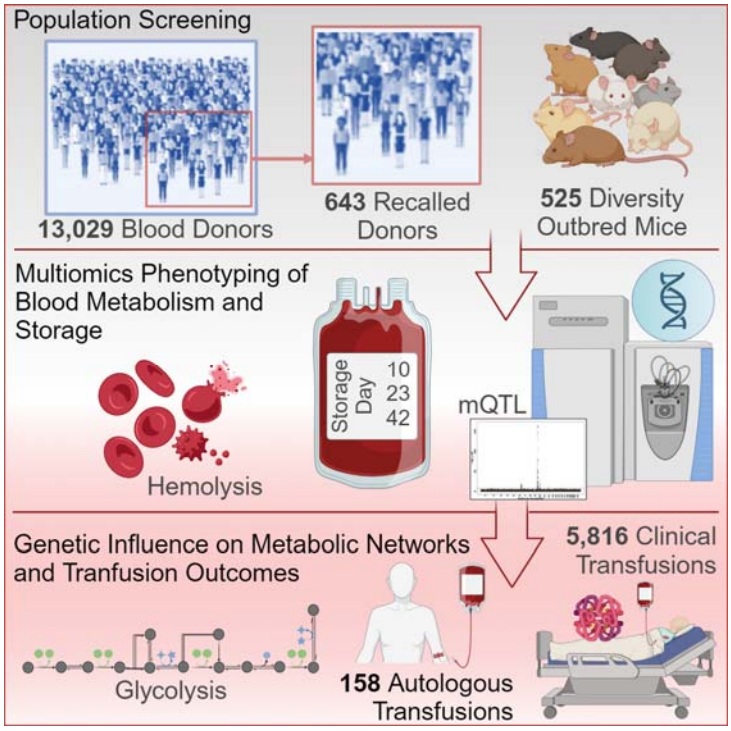

Summary

Mature red blood cells (RBCs) lack mitochondria, and thus exclusively rely on glycolysis to generate adenosine triphosphate (ATP) during aging in vivo and during storage in vitro in the blood bank. Here we identify an association between blood donor age, sex, ethnicity and end of storage levels of glycolytic metabolites in 13,029 volunteers from the Recipient Epidemiology and Donor Evaluation Study. Associations were also observed to ancestry-specific genetic polymorphisms in regions coding for phosphofructokinase 1, platelet – which we detected in mature RBCs - hexokinase 1, and for the ADP-ribosyl cyclase 1 and 2 (CD38/BST1). Gene-metabolite associations were validated in fresh and stored RBCs from 525 Diversity Outbred mice, and via multi-omics characterization of 1,929 samples from 643 RBC units during storage. ATP levels, breakdown and deamination into hypoxanthine were associated with hemolysis in vitro and in vivo, both in healthy autologous transfusion recipients and in 4,700 heterologous critically ill patients.

Highlights

- Blood donor age and sex affect glycolysis in stored RBCs from 13,029 volunteers;
- Ancestry-based genetic polymorphisms in PFKP and CD38/BST1 influence glycolysis in stored human and fresh or stored murine RBCs;
- PFKP is detected in pure mature RBCs and boosts glycolytic fluxes when ATP is low, such as in stored RBCs;
- ATP and hypoxanthine associate with RBC hemolysis in vitro and in vivo in mice and thousands of transfusion recipients.

Keywords

Erythrocyte; Embden-Meyerhof-Parnas; Blood; ATP; Hemolysis;

INTRODUCTION

Red blood cells (RBCs) comprise ~83% of all cells in the human body[1]. Unlike other vertebrates,[2] mammalian RBCs evolved to maximize oxygen carrying capacity by increasing hemoglobin content per cell, a feature achieved by discarding nuclei and organelles, including mitochondria. As such, mature RBCs are completely reliant on glycolysis for the generation of adenosine triphosphate (ATP). ATP fuels all key processes in mature RBCs, from proton pumps[3] to membrane integrity via phosphorylation of structural proteins,[4] from protein stabilization via fueling of transglutaminase 2[5] to cellular mechanics[6], from cytoskeletal actin polymerization[7] to vesiculation[8], from membrane regulation of lipid asymmetry by fueling phosphatidylserine flippases[9] to proteasomal activity to remove damaged proteins.[10] It has long been posited that the ATP-depleted erythrocyte is rapidly removed from the bloodstream[11] via mechanisms of intra- or extravascular hemolysis, such as sequestration in the splenic slit and erythrophagocytosis by resident macrophages in the reticuloendothelial system[3].

Given the lack of *de novo* protein synthesis capacity, RBCs rely on dynamic metabolic reprogramming in response to environmental stimuli, including hypoxia or oxidant stress (e.g., altitude, exercise or storage in the blood bank)[12]. Generation of high-energy phosphate compounds ATP and 2,3-bisphosphoglycerate (BPG) is also central to RBC capacity to perform their main task, i.e., oxygen transport and delivery to tissues that, unlike RBCs, rely on oxygen as a final acceptor of electrons to sustain mitochondrial metabolism. Specifically, ATP and BPG play critical roles in hemoglobin allostery[13] by stabilizing the tense deoxygenated state and promoting oxygen release to tissues[11].

Ease of collection and shear abundance have made RBCs an attractive model for investigating metabolism since the early days of biochemistry.[14] Relevant to biology at large, mitochondria-devoid RBCs represent a simplified model of eukaryotic cell metabolism, a cell type that exclusively relies on glycolysis as the main source of energy for the synthesis of ATP. For the reasons above, it is not a coincidence that the earliest efforts to reconstruct human metabolic networks in silico have been centered on RBC metabolism[15]. A culmination of nearly a century of studies involving many pioneers in the burgeoning field of biochemistry[16], glycolysis, or the Embden-Meyerhof-Parnas pathway explained the cell's ability to convert glucose into ATP even in the absence of oxygen[17]. Despite the importance of metabolism and glycolysis in health and disease, and decades of research on the biochemical determinants of glycolytic fluxes in mammals[18], understanding glycolytic regulation in mature RBCs holds relevant implications for systems physiology and clinical practice. Indeed, in addition to the central role RBCs play in mediating systemic gas and metabolite exchange throughout the body, understanding erythrocyte metabolism

holds the key to optimizing storage conditions and predicting post-transfusion performance of blood products[19].

Transfusion of packed RBCs (pRBCs) is the most common in-hospital medical procedure after vaccination, a life-saving intervention for tens of millions of civilian and military patients whose survival depends solely on chronic or massive transfusions, with no current alternative medical interventions. Altered energy metabolism is a hallmark of the so-called storage lesion,[20] a series of biochemical and morphological alterations that ultimately increase the propensity of stored RBCs to hemolyze ex vivo in the refrigerated unit or in vivo upon transfusion. Biopreservation of leukocyte-filtered pRBCs for up to 42 days at 4ºC poses an energetic challenge to erythrocytes, as proton pumps fail under refrigerated storage temperatures and become a sink for ATP consumption.[20] Storage-dependent consumption of glucose is not limited by its availability in currently licensed storage additives, which contain supra-physiological concentrations of glucose in all the most common additives (e.g., 111 mM and 55 mM for additive solution 1 and 3 in the United States – AS1 and AS3, respectively)[21]. As storage progresses and glucose is metabolized through glycolysis, lactic acid accumulates up to 35 mM in the closed system of a blood bag,[22] with a concomitant drop in pH.[23] Intracellular acidification has a negative inhibitory feedback on pH-dependent enzymes, such as phosphofructokinase (PFK), bisphosphoglycerate mutase (BPGM), and glucose 6-phosphate dehydrogenase (G6PD), the rate-limiting enzymes of glycolysis, the BPG-generating Rapoport-Luebering shunt and the pentose phosphate pathway (PPP), respectively.[24] Combined with slower than physiological enzyme kinetics at 4ºC (compared to 37ºC *in vivo*),[25] ATP synthesis rate become insufficient to sustain fueling of proton pumps. As a result, BPG pools (~5 mM) rapidly deplete to promote compensatory ATP synthesis, with BPGM phosphatase activity favored over its kinase one by the drop in pH.[24] As adenylate pools shift to lower energy adenosine monophosphate (AMP) and adenosine, BPG-depletion and oxidant stress both contribute to activate adenosine/AMP deaminase 3[26,27], which ultimately generates hypoxanthine,[25,26,28,29] a key hallmark of the metabolic storage lesion[20]. Although the clinical relevance of the storage lesion remains unresolved – which is, in part, the focus of this study - it is now clear that RBC metabolism under refrigerated storage conditions is impacted by storage temperatures, additive solutions, donor dietary or other exposures (e.g., smoking, alcohol consumption, drugs that are not grounds for blood donor deferral), and also by factors such as donor age, sex, ethnicity and body mass index (BMI).[25,26,28-30] While it has been posited that RBC storability and post-transfusion performance are a function of donor genetics[31] and non-genetic factors[32], the biological and genetic underpinnings of RBC glycolysis have not yet been determined, since no study to date was sufficiently powered to

test the independent and combined contributions of these factors from an omics standpoint, which is the central focus of this study.

Current gold standards of storage quality are the measurement of (i) "in bag" hemolysis (i.e., the percentage of RBCs that lyse spontaneously by storage in the blood bank for 42 days) and (ii) post-transfusion recovery (PTR) with radiolabeled ^{51}Cr studies in healthy autologous recipients, which measures the percentage of stored RBCs that still circulate in the bloodstream of the recipient 24h after transfusion. The FDA and European Council have identified <1% and >75% thresholds for end of storage hemolysis and PTR, respectively, as the gold standards of quality for the last several decades. However, these are limited to licensing of new products, as they are not routinely performed on all products issued for transfusion, owing to technical and economic considerations. In addition, both metrics have major limitations,[33] and inter-donor heterogeneity in these parameters has been noted for both.[34-36] Finally, neither of these "quality" testing parameters provides any insights regarding preservation of RBC "function" upon storage, which is a critical unmet clinical need. For these reasons, both the National Heart, Lung and Blood Institutes[37] and the Food and Drug Administration (FDA)[38] have listed the identification of new functional biomarkers of RBC storage quality and post-transfusion performances as central to their programmatic agenda.

The recent implementation of high-throughput and cost-effective genomics and metabolomics platforms has enabled powerful large scale metabolic Quantitative Trait Loci (mQTL) studies[39]. This new body of work has extended Garrod's classic concept of chemical individuality[40], through comprehensive genome-wide association studies that reveal how genetic variation contributes to the heterogeneity of blood metabolite levels[41]. Most of these studies have interrogated the genetic underpinnings of pathological metabolic conditions by focusing on serum/plasma fractions of the circulating metabolome. These efforts underlie the foundation of modern day clinical chemistry, especially the focus on inborn errors of metabolism, including those linked to hemolytic disorders (e.g., pyruvate kinase deficiency,[42] glucose 6-phosphate dehydrogenase deficiency[43]).

Herein we build upon these efforts by leveraging a combination of genomics and ultra-high-throughput metabolomics approaches (1 min per sample) to test the specific hypothesis that donor biology, including age, sex and genetic ancestry play a role in regulating stored RBC glycolysis. One corollary to this hypothesis is that, given the role of glycolysis in ATP (and, indirectly, BPG) synthesis in mature RBCs, and the role of these molecule(s) regulating RBC biology and function with respect to O_2 homeostasis, biological and genetic factors that affect glycolysis of stored RBCs ultimately underlie RBC hemolytic propensity, either "in the bag", or in the circulatory system of the recipient following transfusion. In summary, the present study addresses knowledge gaps that

remain in the understanding of how biological and genetic factors impact RBC storage biology and transfusion outcomes.

RESULTS

Glycolysis is influenced by donor sex, age, ethnicity and BMI

To bridge these gaps, first we performed high-throughput metabolomics analyses on leukocyte-filtered pRBCs, which were donated by 13,029 volunteers at four different blood centers across the United States and stored for 42 days (i.e., at the end of the FDA-approved shelf-life - **Figure 1.A**). All raw and processed data (normalized to plate medians), as well as principal component analyses of pre- and post- normalization, and detailed information of metabolite IDs (KEGG or HMDB), m/z retention times and adducts are provided in **Supplementary Table 1**. The donor population was balanced with respect to sex (6,507 males and 6,522 females) and blood center (from a minimum of 3,019 to a maximum of 3,564 per center). The age range spanned from 18 to 87 (median age 47) with median body mass index (BMI) of 26.6. Most donors were of Caucasian descent (7,037), with substantial representation of individuals of Asian (1,602), African (1,542) and Hispanic descent (1,153) and Other (including multiracial people, Alaska/Hawaiian/Native Americans, and Pacific Islanders – 1,695). Additive solution 1 (AS-1) and AS-3 were the only additives used (their compositions are detailed in **Supplementary Table 1**). Linear discriminant analysis (LDA) of all the samples as a function of donor age, sex, body mass index (BMI) and ethnicity identified strong effects of each factor on the metabolic heterogeneity of end of storage pRBC units (**Figure 1.B-E)**.

Unsupervised uniform manifold approximation and projection (uMAP) was then used to cluster the 13,029 samples based on metabolic phenotypes alone, which highlighted a group of donors with elevated ATP (**Figure 1.F**). We thus set out to determine the biological characteristics of this group of donors with high ATP. First, we observed that donor age and sex had the strongest effect on RBC glycolysis, followed by donor ancestry, with a less marked effect of BMI (**Supplementary Figure 1**). Younger donors had significantly higher levels of ATP, which was negatively associated with donor age, independently of sex, with lowest levels observed in morbidly obese donors (BMI>40); higher levels of ATP were instead observed in donors of Hispanic descent (Mexican and Central American Hispanics) even at older ages (**Figure 1.G**). Lactate was higher in older donors age, with highest levels in male donors of Caucasian, East Asian or Other descent. Results clearly show a progressively lower levels of ATP and all glycolytic intermediates, but higher levels of lactate as a function of donor age (**Supplementary Figure 1.A**). Despite consistent age-associated trends for all donors, sex dimorphism was observed, with lower levels of glucose and

higher levels of glycolytic metabolites in males across the age range (e.g., BPG, phosphoenolpyruvate - PEP and lactate, but not ATP). Dimorphism in the levels of glucose and glycolytic metabolites was lost for donors past 50 years of age, the average age of menopause in the United States [44] (**Supplementary Figure 1.B**). RBCs from donors with the highest BMIs (morbidly obese; >40) were characterized by significantly higher levels of lactate, as compared to all the other BMI groups within the age window of 30-60 (**Supplementary Figure 1.C**).

Unsupervised clustering separates donors with high glycolysis from the rest of the donor population

We then performed K-means clustering to identify data-driven unsupervised donor clustering based on metabolic patterns of end of storage units: this analysis clearly identified cluster 4 as the most distant cluster from the rest of the population (**Figure 1.H**). Of note, donors in this cluster matched the donors with the highest levels of ATP in the uMAP analysis in **Figure 1.F.** Network analysis of metabolite-metabolite correlations across each cluster (**Figure 1.I**) and through the whole population (**Figure 2.A**) revealed a central core of metabolites involved in glycolysis, significantly associated to donor demographics, especially age and sex (**Figure 2.A**). Hierarchical clustering analysis of samples based on the top 50 significant metabolites that discriminate the 10 K-means clusters by ANOVA detected a strong signal separating donors in cluster 4 from the rest (highlighted in red in **Figure 2.B**). These results indicated a metabolic rewiring in glycolysis for samples in cluster 4, which were characterized by the highest levels of ATP through the whole donor age range (**Figure 2.C**), suggesting that higher ATP levels in this group are not exclusively explained by donor age. Donors in cluster 4 also showed elevated levels of all glycolytic metabolites (**Figure 2.D**), which all positively correlated to ATP levels (**Supplementary Figure 2**). Of note, hypoxanthine (HYPX) – a breakdown and deamination product of ATP – was the top negative correlate to ATP levels (**Supplementary Figure 2.D**). Donors with the highest levels of ATP, either alone or in combination with the lowest levels of hypoxanthine (**Supplementary Figure 2.A-D**) showed markedly distinct end of storage metabolic phenotypes, especially elevated glycolysis (**Figure 2.D**). Interestingly, donors in clusters 4 were overall younger, leaner (lower BMI), with a highly proportion of male donors compared to the other clusters combined (**Figure 2.E**). These units were mostly stored in AS-3 (87%) versus AS-1 (13%), while the rest of the population had a comparable balance (51 vs 49%) between the two additives (**Figure 2.E**). We[22,45-48] and others[25,28,29,49] have extensively investigated the impact of storage additives on the heterogeneity of stored RBC units.[45] Consistent with the literature and the composition of the additives (e.g., violin plots for metabolites included in additive formulations are shown next to the licensed composition in **Supplementary Table 1**), higher glucose levels in AS-3 were associated

with higher levels of ATP, BPG and all glycolytic metabolites for donors of all ages, with the exception of lactate (**Figure 2.F**). This observation is relevant in that it differs from observations based on donor demographics (e.g., age, sex, ethnicity), for which ATP, glycolysis and lactate levels were concordant (e.g., all glycolytic metabolites downstream to BPG all the way to lactate were higher in males than females – **Supplementary Figure 1.B**). Thus, additives alone are insufficient to explain the boost in glycolysis. Indeed, while RBCs from donors in cluster 4 were more likely to be stored in AS-3 than in the other clusters, only 360 units in this group were stored in AS-3, against a residual 6378 from all the other groups combined (**Supplementary Table 1**). Altogether, our data are the first to describe that higher levels of ATP are detected in end of storage units from younger, male donors stored in AS-3 in the largest donor population assessed to date, and that this results in a lower incidence of storage hemolysis (**Figure 2.E**). We also observed that donors in cluster 4 were less diverse than the rest of the REDS donor population, as they were significantly enriched in donors of Caucasian descent, with significantly lower representation of donors from other ancestries (**Figure 2.E**)

By study design, the REDS RBC Omics project included a validation phase in which 643 donors out of the 13,029 donor index cohort were selected based on their hemolytic propensity. Specifically, donors who ranked in the 5th or 95th percentile for end of storage measurements of hemolysis were invited to donate a second unit of blood, which was again tested for hemolytic propensity[35] and multi-omics analyses at storage days 10, 23 and 42.[50] Consistent with a donor-dependency of glycolysis (at the biological and genetics level), the steady state abundance of glycolytic metabolites at storage day 42 was significantly reproducible across multiple donations from the same donors who were enrolled in both the index and recall phase of the REDS RBC Omics study (examples for glucose, hexose phosphate, lactate are in **Supplementary Figure 2.F)**. Altogether, these results suggest a potential impact of genetics on stored RBC glycolysis, in addition to biological factors.

Genetic underpinnings of glycolytic heterogeneity in fresh and stored murine RBCs in the J:DO study

To delve into the genetic underpinnings of metabolite changes while controlling for biological (sex, age, BMI) and processing factors (storage additives), we measured metabolite levels in fresh and stored murine RBCs from 525 mice from the Jackson Laboratory's Diversity Outbred (J:DO) mouse population. Murine RBCs were stored for 7 days, which was chosen following pilot studies aimed at identifying a storage range that resulted in end of storage PTR comparable to humans[51], while also accounting for the wide variability in PTR amongst the J:DO founder mouse

strains. Briefly, eight genetically diverse founder strains were crossed for >46 generations to establish this population with highly recombined genomes (**Figure 3.A**). These mice were genotyped on a genotype array with 137,192 markers, fresh and stored RBCs were tested for the levels of glycolytic metabolites, and results were adjusted for sex and cage batches (**Figure 3.A**). These analyses identified key regions of co-mapping metabolite quantitative trait loci (mQTLs) on murine chromosomes 5 and 13 for ATP levels and glycolytic metabolites, as highlighted by Manhattan plot, hive plot and heat map illustrations (**Figure 3.B-D**). Representative Manhattan plots, founder haplotype effects and locus zoom plots are shown for ATP and fructose bisphosphate (BP) in **Figure 3.E-H**. Altogether, these analyses associate ATP and glycolytic metabolites with a polymorphic region on chromosome 5 which encodes for the ectonucleotidase CD38, also known as ADP-ribosyl cyclase 1, or the neighboring bone marrow stromal antigen - BST1 (also known as CD157), an ectonucleotidase with similar activity to CD38. BST1 is a pH-dependent NAD(P)+ hydrolase, also known as ADP-ribosyl cyclase 2.[52,53] Our analyses also identified an association of glycolytic metabolites and ATP to a second region on murine chromosome 13, which encodes phosphofructokinase platelet - PFKP (**Figure 3.G**). The CD38 region associated with all glycolytic and PPP metabolites in stored and fresh murine RBCs, while the PFKP region only associated with stored RBCs (**Figure 3.B;** in **Supplementary Figure 3**).

Of note, a preliminary analysis of a smaller subset of 350 animals from this diversity outbred mice cohort did not identify any significant mQTL near PFKP. Subsequent analysis of the total cohort of 525 animals resulted in the detection of mQTL near PFKP for multiple metabolites, including fructose bisphosphate (**Figure 3.G-H**) and erythrose phosphate (**Supplementary Figure 3.A**), but only when murine RBCs were stored. Haplotype effects in this region in the BST1/CD38 region reveal for high alleles inherited from NZO/ HlLtJ, PWK/ PhJ, and WSB/Eij for ATP (**Figure 3.F**), which are inverted for Glyceraldehyde 3P (**Supplementary Figure 3.E**) in stored RBCs. Haplotype effects for the mQTL in the PFKP region for fructose bisphosphate in stored RBCs (**Supplementary Figure 3.B**) are more complex and distinct from the CD38 region.

As a first validation of the mouse results in humans, the CD38 SNP rs4478185 in the REDS RBC Omics Index cohort, while rare (homozygous recessive in 0.2% and heterozygous in 3.4% of the index population), was significantly associated with levels of glycolytic metabolites and ATP (**Figure 3.I**). As a reassuring internal validation of the quality of the metabolomics data, we observed a positive association of this SNP with $NAD(P)^+$, and a negative association with nicotinamide and ADP-ribose, substrates and products, respectively of the enzymatic activity of CD38 (**Figure 3.I**). Indeed, mQTL analysis for ADP-ribose highlighted both CD38/BST1 and

PFKP SNPs as top loci associated with the end of storage levels of this metabolite in the index donor population (**Figure 3.I**).

Genetic polymorphisms associated with the glycolytic heterogeneity of end of storage units from 13,029 REDS RBC Omics Index donors

To help further translate these murine findings into the human settings, we tested the 13,029 REDS Index donors for ~879,000 single nucleotide polymorphisms (SNPs), which enabled mapping of mQTL (**Figure 4.A**). For these genome-wide association studies, metabolomics data were adjusted for donor sex and age, BMI and storage additives. A full list of the gene-metabolite associations also includes a comparison of findings from the present study against the GWAS catalogue[54] (**Supplementary Table 1**). Many of the "hits" that had already been described in the literature pertain to hematological parameters, such as RBC count, hematocrit, platelet (PLT) count, and hemoglobin concentration (**Supplementary Table 1**). A summary Manhattan plot of mQTL results is shown for all glycolytic metabolites merged together (**Figure 4.B**), or just for ATP (**Figure 5** and **Supplementary Figure 4**). Manhattan plots are also shown for lactate (**Figure 4.B**) and each of the glycolytic metabolites (**Figure 4.C-J**). A similar analysis was performed for the PPP end product, pentose phosphate (PP - including ribose phosphate and other pentose phosphate isomers that are not resolved by the high-throughput assay). Related locus zoom plots for the most common SNPs in PFKP (chromosome 10) that associate with ATP and lactate (FDR-corrected p-value = e-163) are in **Supplementary Figure 5.** Of note, SNPs in PFKP also ranked as the strongest factors influencing hypoxanthine levels, followed by SNPs in the region coding for adenosine deaminase (ADA, chromosome 20 – **Figure 4.C**), which catalyzes the deamination of adenosine to inosine, that then undergoes hydrolysis to hypoxanthine; and inosine triphosphate pyrophosphatase (ITPA, chromosome 20 – **Figure 4.C**), which catalyzes ITP to inosine monophosphate, a precursor to hypoxanthine.

This analysis also identified multiple common hot spot areas in regions coding for other rate-limiting enzymes of glycolysis,[18] hexokinase 1 (HK1, chromosome 10), phosphofructokinase M (PKFM, chromosome 12), pyruvate kinase (PKLR, chromosome 1), or other enzymes involved in glucose 1,6-bisphosphate metabolism (phosphoglucomutase 2 like 1 - PGM2L1, chromosome 11 – **Figure 4.C** and **I**). Similarly, end of storage levels of pyruvate showed a strong association with the X-linked rate-limiting enzyme of the PPP, glucose 6-phosphate dehydrogenase (G6PD –**Figure 4.D**). For hexose phosphate, an extremely significant hit (p<e-300) was observed on fructosamine 3-kinase (FN3K). For glycolytic metabolites downstream to glyceraldehyde 3-phosphate, a common hit - absent in the hexose phosphate group - was the CD38/BST1. Both CD38 and BST1 map on

human chromosome 4, and multiple distinct loci in this region were linked to different metabolites such as ADP-ribose or pentose phosphate (**Supplementary Figure 5.B-C**). As anticipated above, the CD38 findings for metabolites downstream to glyceraldehyde 3-phosphate in glycolysis and PPP metabolites were consistent between the J:DO mice and humans (**Supplementary Figure 3.F-G** shows two representative locus zoom comparisons for murine – top – and human – bottom – glyceraldehyde 3-phosphate). For glyceraldehyde 3-phosphate and ribose phosphate, a hit on RHCE (chromosome 1) suggests a potential cross-talk between the RH blood group components and the metabolic steps linking the non-oxidative branch of the PPP to triose phosphate compounds (**Figure 4.G**). HSB1L-MYB (chromosome 6) was linked to phosphoglycerate (**Figure 4.H**) and CPPED1 (chromosome 16) to phosphoenolpyruvate (**Figure 4.I**). PKLR association to hypoxanthine, phosphoglycerate and phosphoenolpyruvate in stored human RBCs (**Figure 4.B, H-I**) found correspondence in stored, but not fresh murine erythrocytes for BPG and phosphoenolpyruvate, owing to alleles carried by PWK and WSB mice (**Supplementary Figure 3.H-I; Supplementary Table 1**).

Glycolytic heterogeneity and donor genetic ancestry

A summary overview of the gene-metabolite associations is shown as a circos plot in **Figure 5.A**. To further expand on the mQTL analyses, we determined mean allele frequency for different genetic ancestry groups (**Supplementary Table 1**). Results are summarized in the form of gene-metabolite network plots (red-blue, respectively) for the whole population, and broken down by genetic ancestry (**Figure 5.B**); these showed that – despite Caucasian donors representing more than half of the population in this study – donors of African and Hispanic descent and, to a lesser extent, of Asian descent were still characterized by complex associations between genes and glycolytic metabolites. For example, the ATP-PFKP association (**Figure 5.C -** list of the top 10 SNP by adjusted p-value in **Supplementary Figure 4.D**; full list in **Supplementary Table 1**) was the strongest in Caucasian donors, and almost completely disappeared and lost significance in donors of Hispanic and African descent, while it was not observed in donors of Asian ancestry (**Figure 5.D**). In contrast, some associations (e.g., hexose phosphate and FN3K) were extremely significant across all donor ancestries, with strongest signals in donors of Caucasian and Asian descent, followed by Hispanic and African donors. Similarly, the PFKP-lactate association was observed and comparably significant across all ancestries (**Figure 5.F**). Finally, some gene-metabolite associations were unique to specific groups. For example, the association between pyruvate and G6PD (rs1050828, c.202G>A; p.Val68Met), known as the African variant[43] was observed exclusively in donors of

African descent and, to a lesser extent, in Asian donors. An overview of all observed gene-metabolite associations is provided in **Figure 5.H**

Interactions between PFKP polymorphisms and donor age, sex and ethnicity in index and recalled human donors

Correlation analysis of the allele frequency for the top PFKP SNP associated with glycolysis (rs2388595) confirmed a strong positive association with lactate and a negative association with hypoxanthine levels (**Figure 5.I**), and overall impacted all glycolytic metabolites (**Supplementary Figure 5.B**). The frequency of PFKP rs2388595 homozygosity was highest in donors of Caucasian (25%) or Asian descent (23%), and lowest in donors of Hispanic descent (18% - **Supplementary Table 1**). Effects of biological variables, such as donors age and sex were further enhanced by PFKP SNPs, especially with respect to glucose and fructose 1,6-bisphosphate consumption and lactate accumulation, with concomitantly lower levels of hypoxanthine in older male donors who carry two alleles of the PFKP rs2388595 SNP (**Supplementary Figure 6.D-E**). While no significant interaction effects were observed, the influence of biological variables such as age and sex further impacted metabolite levels in the context of PFKP SNPs, especially with respect to glucose and fructose bisphosphate consumption and lactate accumulation, with concomitantly lower levels of hypoxanthine in older male donors carrying two alleles of PFKP SNP rs2388595 (**Supplementary Figure 6.E**), as highlighted by the following fitting model: Metabolite X ~ Age x SNP x Sex + HUB + DonFreq (**Supplementary Figure 4.G; Supplementary Table 1**).

To validate and expand on these genomics and metabolomics findings, we performed proteomics analyses on 1,929 samples at storage day 10, 23 and 42 from longitudinal sampling of a second, independent unit from donors recruited in the recalled donor cohort (**Supplementary Table 1**). These analyses showed that PFKP protein levels ranked as the top positive correlate to PFKP rs2388595 allele dosage, suggesting that this intronic variant impacts protein expression (**Figure 5.J**). No association was observed for any PFK isoform with donor age and sex (**Supplementary Figure 6.F**). Since PFKP is a platelet (PLT)-specific isoform, we questioned whether our omics measurements and mQTL results had been influenced by changes in cellular blood counts and PLT contamination. However, we found no association between ATP measurements and RBC or PLT counts at the time of donation, nor between PFKP SNP or PFKP protein levels and PLT counts (**Supplementary Figure 7.A-C**). Whereas the tested RBC units from the donors enrolled in REDS were buffy coat depleted and leukoreduced by filtration, which removes log4 and log2.5 white blood cells and platelets,[35] respectively – a standard workflow in RBC manufacturing in most states in the United States of America – we questioned whether detection of PFKP in mature RBC was

attributed to PLT contamination. As such, we performed a separate preparation of ultra-pure mature RBCs from 5 independent volunteers, whose blood was leukofiltered and flow-sorted to remove WBCs, PLTs and immature reticulocytes (based on CD41, CD45, CD62P, and CD71 cell surface markers) and positively enriched for CD235a^{+} CD71^{-} mature RBCs (**Supplementary Figure 7.D**). Proteomics analyses of the pure mature RBC population still identified PFKP, which comprised ~11% of total PFK isozyme population – ~89% of which represented by PFKL/M (**Supplementary Figure 7.E**). The RBC proteome did not change significantly in these samples, neither as a function of storage or as a function of PFKP allele dosage (**Supplementary Figure 7.F**).

Dynamic modeling of PFKP in stored RBCs

Linear discriminant analysis of proteomics data (**Figure 6.A**) further corroborated correlation analyses (**Figure 5.J**), both indicating that protein levels of PFKP are the most significant variable associated with the mean allele frequency for SNP rs2388595, even after adjustment of proteomics data for storage duration and donor age or sex. Specifically, proteomics data showed a ~30% increase in PFKP protein levels in donors carrying two alleles of this SNP (**Figure 6.B**). RBCs from these donors were also characterized by significantly higher levels of GAPDH, and higher medians (albeit not significant) for LDHB as a function of allele dosage (i.e., lowest in 0 copies – here defined as homozygous dominant or HD; intermediate with 1 copy – heterozygous or HET; highest with two copies – homozygous recessive or HR – **Figure 6.B**). To expand on steady state measurements at storage day 42 from index donors (**Figure 1; Supplementary Figure 1**) and day 10, 23 and 42 from recalled donors (**Supplementary Figure 6.F**), we then performed a storage experiment using 6 new units of pRBCs, which were sterilely sampled weekly to obtain a more granular understanding of the progression of the metabolic storage lesion to glycolysis (**Figure 6.C**). The results indicated a drop in ATP, down to 20% of the initial levels by storage day 42. These analyses were then complemented by a separate identical experiment, in which the units were spiked with 1,2-$^{13}C_2$-glucose, to measure trace ^{13}C into glycolytic intermediates all the way to lactate as percentage of the total isotopologue levels throughout storage (**Figure 6.D**). These combined analyses show that glycolytic fluxes are active during storage, that FBP and lactate are ~100% and ~90% labeled by the end of storage, and that de novo BPG synthesis occurs during the first two weeks of storage but is insufficient to maintain the BPG pools; finally, the PFK-catalyzed step appears to be rate-limiting, since FBP declines at the fastest rate of all glycolytic metabolites despite ongoing synthesis, (**Figure 6.C-D**).

To understand the role of the PFKP isozyme in human RBCs, we reconstructed a mass action stoichiometric simulation model of the in vivo RBC glycolytic pathway at steady state[55,56]. Previous

in vitro and in silico studies on PFK isozymes suggest that there are distinct metabolic roles for each isozyme due to differences in kinetic and regulatory properties, and that the simultaneous expression of the different isozymes consequently expands the cell's metabolic capacity to respond to various conditions[57,58]. In particular, PFKP is notable among PFK isozymes as it is not allosterically activated by either fructose 1,6-bisphosphate or glucose 1,6-bisphosphate. Furthermore, PFKP has the lowest affinity for ATP as a substrate and a relative insensitivity for inhibition by ATP, suggesting that it would be the most responsive of these isozymes when ATP concentration is low.

Therefore, we replaced mass action rate laws with detailed enzyme kinetic equations and parameters for the key regulatory enzymes hexokinase, phosphofructokinase, and pyruvate kinase[59,60], ensuring their regulatory properties were represented in the model. Differences in glycolytic enzyme abundances were calibrated on the experimental proteomics data for stored RBCs donated by volunteers carrying 0 or 2 alleles of PFKP SNP rs2388595 (HD vs HR, respectively – **Figure 6.B**). We then assumed that the existing PFK reaction was catalyzed by the tetrameric enzyme formed by liver and muscle isozymes in erythrocytes – the most abundant isoforms based on our proteomics analyses (~89% - based on **Figure 6.B**). Total PFK abundance was set to 1e-7 M[61], with PFKP accounting for ~11% of the total PFK isozyme (based on **Supplementary Figure 7.E**), and modeled a ~30% increase in PFKP levels in HR donors vs HD (based on **Figure 6.B**). Mature RBCs cells do not contain significant concentrations of fructose 2,6-bisphosphate[22,25,29,49]; therefore, we assumed that fructose 2,6-bisphosphate is negligible as an effector in the intracellular RBC environment.

Finally, we created a second version of the model and modified it with a second PFK reaction to represent the PFKP isozyme. We parameterized the PFKP isozyme in the model relative to the PFKL isozyme from true comparative and protein structure studies where possible to avoid discrepancies due to different assay conditions across studies[57,62-64]. Models representing RBC glycolysis with and without PFKP were simulated after a sudden 80% decrease in ATP concentration – consistent with changes observed in stored RBC after 42 days of storage (based on **Figure 6.C**) - to provide insight into the role of PFKP in the recovery of cellular ATP. Glycolytic fluxes were then modeled over a time scale of 10^{-4} to 10^{4} seconds prior to and after the simulated drop in ATP over storage (**Figure 6.E**). The simulation shows that, upon the perturbation of ATP pools, dynamic changes in glycolytic fluxes (+30%), PFKM and PFKP activities, and total energy charge are observed (**Figure 6.E**; **Supplementary Figure 7.G**)). Early glycolytic metabolites that are substrates for and products of PFK activity, such as fructose 1,6-bisphosphate levels (**Figure 6.F**) and adenylate pools (AMP+ADP+ATP – AxP – **Figure 6.G**), were estimated to be ~30%

higher in donors expressing higher levels of PFKP (HR group). This simulation is consistent with previous models in other cellular systems [57], suggesting that kinetic and regulatory properties of each isoform make PFKP responsive in low ATP conditions, and PFKL in low F6P conditions (**Figure 6.H**). As such, the simultaneous expression of both isoforms expands the metabolic capacity for the F6P to FBP reaction under varying conditions (**Supplementary Figure 7.H**).

RBCs from donors with high end of storage ATP and low hypoxanthine are characterized by lower hemolysis in vitro and in vivo in healthy and critically ill recipients of autologous or non-autologous transfusions, respectively

End of storage spontaneous hemolysis in the bag was measured in 12,753 units from the REDS RBC Omics index donor cohort (**Figure 7.A**). High levels of ATP and glycolytic metabolites in cluster 4 were associated with significantly lower levels of hemolysis (**Figure 7.A**), as were units from donors carrying two alleles for the SNP rs2388595 (**Figure 7.B**). However, in vitro hemolysis was a poorly sensitive marker of unit quality, since >97% of units (independent of cluster or genotype) had less than 1% hemolysis. As such, we focused on the other quality gold standard, PTR. Specifically, we determined metabolic correlates to PTR in a separate cohort of 79 volunteers from the Donor Iron Deficiency Study (DIDS) of frequent donors (**Figure 7.C**).[65] From this analysis, glycolytic metabolites and ATP and hypoxanthine levels were positively and negatively correlated with PTR, respectively, in healthy volunteers receiving autologous ^{51}Cr-labeled RBCs (**Figure 7.C**). By accessing the "vein-to-vein" database of the REDS RBC Omics program, we first linked blood donor PFKP SNPs to decreases in adjusted hemoglobin increments as a function of allele frequency for rs2388595 (and the strongly positively correlated rs61835134 by allele dosage - r = 0.93 in **Supplementary Table 1**), in patients receiving single irradiated RBC units (**Figure 7.D**). We then linked ATP and hypoxanthine levels to hemoglobin increments (n=5,816 records available in the database) and bilirubin increments (n=914) upon transfusion of heterologous products from REDS donors to ill recipients requiring transfusion (**Figure 7.E**). Results indicate a significant positive association between ATP levels and hemoglobin increments in transfusion recipients, along with decreased bilirubinemia (i.e. lower hemolysis in vivo) in patients receiving these units. In addition, the opposite results were observed as a function of hypoxanthine levels, yielding lower hemoglobin increments and higher bilirubin increments (**Figure 7.E-F**).

DISCUSSION

Herein we report the largest metabolomics study to date of stored RBCs from 13,029 donor volunteers. Our results show that end of storage units are metabolically heterogenous. Specifically, we identified a cluster of donors – younger, male, leaner and predominantly Caucasian - whose RBCs are characterized by elevated glycolysis and ATP levels, and low hypoxanthine levels. Units from these donors also exhibited lower hemolysis in vitro and in vivo, and were associated with higher hemoglobin increments in patients transfused with units from these donors. As an internal quality control measure of the metabolomics and genomics data from this cohort, mQTL analyses identified common polymorphisms in PFK (PFKP more significantly than PFKM) and HK1, which are well-established rate-limiting enzymes of glycolysis,[18] and reveal themselves as the main genetic contributors to the glycolytic heterogeneity in stored human RBC units. While PKFP SNPs were previously associated with PLT counts in the GWAS catalogue, [54] here we did not observe an association with PLT (or RBC) count and PFKP protein or ATP levels. Nonetheless, proteomics analyses of ultra-pure RBC populations confirmed that PFKP is, indeed, expressed in mature erythrocytes, accounting for ~11% of total PFK isoforms. Lactate levels were also associated with to PFKM SNPs, including with the missense mutation Gln76Lys (rs4760682), although with a much lower significance (p=e-11 instead of e-163), likely owing to the lower mean allele frequency of this variant in the REDS donor population.

RBC units from these donors were also primarily stored in AS-3, an additive that is high in citrate to compensate for the lack of mannitol as an osmoprotectant. This formulation was designed to mitigate osmotic stress that lead to elevations of intracranial pressure in recipients, making this additive appropriate for pediatric patients and patients with traumatic injury.[47] However, the excess citrate could play a hitherto unappreciated role in the economy of RBC glycolytic fluxes. Previous studies showed that RBCs possess functional cytosolic isoforms of Krebs cycle enzymes that could utilize citrate as a substrate to contribute to NADPH homeostasis (e.g., isocitrate dehydrogenase 1); enzymes in this pathway could also contribute to oxaloacetate and malate pools (via cytosolic malate dehydrogenase 1 and acetyl-coA lyase),[22,29,66,67] ultimately feeding back into late glycolysis at the PEP step by a PEP carboxylase-like mechanism mediated by hemoglobin.[68] The current study offers a different perspective on the intertwining of citrate metabolism and glycolysis in stored RBCs. Specifically, inhibition of PFK activity by citrate is a well-established concept in cells endowed with mitochondria, a process that inhibits glycolysis as a function of fatty acid oxidation – the Randle cycle[69]. The combination of citrate-rich anticoagulants and storage additives would predictably contribute to inhibition of glycolysis through similar effects on PFK activity. However, there are marked dose-response effects for PFKM ($IC_{50}^{citrate}$ 982 ± 109 μM) and PFKP ($IC_{50}^{citrate}$

177 ± 132μM), but not PFKL.[57] Since normal plasma citrate concentrations in humans are within a range of ~100–150μM[70], citrate-dependent isoform-specific regulatory effects on PFK may not only be relevant to the supra-physiological conditions of anticoagulant-supplemented storage additives (up to 25 mM citrate in AS-3), but also in vivo. This consideration may also have implications for the interpretation of citrate as a regulator of immune[71] and cancer[72] cell metabolism, at least in subjects carrying one or two alleles of the PFKP SNPs, i.e., 15% of the donor population in the present study.

Even more interestingly, when specific activities are considered, citrate may no longer act as an inhibitor, but rather as activator of PFK when ATP levels are low (sub-physiological), such as those observed in end of storage RBCs.[57] Such an activating effect is also isoform specific, with PFK-P > PFK-L > PFK-M.[57] Our data and reconstruction simulation perfectly fit with this model, whereby SNPs (such as rs2388595) that are associated with higher expression levels of the PFKP enzyme are also associated with higher glycolytic fluxes in stored human or murine RBCs, but not in fresh murine RBCs. This model not only reconciles the benefits to glycolysis of storage in AS-3, but also provides a plausible rationale underpinning the lack of association between PFKP SNPs and fresh murine RBC metabolism, suggesting that storage-induced ATP depletion in murine and human RBCs is a necessary stress to unmask the PFKP linkage to glycolysis.

Conversely, we identified an association between polymorphisms in the ectonucleotidases CD38 and BST1 – both of which are ADP-ribosyl cyclases (1 and 2) – and NAD(P), PPP, and late glycolysis in both fresh and stored human and murine RBCs. While the literature suggests a role for CD38/BST1 in the regulation of intracellular calcium pools via metabolism of ADP-ribose [73,74], our results do not show a correlation with calcium levels, as measured by ICP-MS. On the other hand, the positive association with ribose phosphate, metabolites in the non-oxidative phase of the PPP and late steps of glycolysis suggest a role for NAD(P) catabolism in stored RBC units as a fuel for ATP synthesis upon phosphorolysis of ADP-ribose and re-entering of the pentose phosphate into glycolysis downstream of glyceraldehyde 3-phosphate.

The mQTL analysis also identified a series of additional novel associations. The most significant of these relates to the association of hexose phosphate and FN3K, a deglycating enzyme and modulator of NRF2 activity in cancer,[75] whose polymorphisms are implicated in the pathogenesis of diabetic complications.[76] Specifically, FN3K catalyzes the phosphorylation of the fructosamine formed upon non-enzymatic reactions of glucose with primary amines, followed by the Amadori rearrangement, thus favoring metabolism of glycation products. Non-enzymatic glycation of proteins is one hallmark of the oxidative stress experienced by stored RBCs,[77] and we previously noted how the supraphysiological glucose concentrations of all currently licensed storage

additives could favor glycated hemoglobin (Hb1Ac) formation similar to that seen in diabetes,[78] though the role of FN3K donor genetics in this phenomenon remains unexplored despite previous association of FN3K SNPs to Hb1Ac levels in the GWAS catalog.[54]

Association between the Rh blood group component RHCE and glycolytic metabolites downstream to glyceraldehyde 3-phosphate and pentose phosphate expands upon a recently described GWAS report[79], as part of which RH components that participates in ammonia transport have been linked to intracellular alkalinization upon exposure to high-altitude. The same SNPs (especially rs1293261) were previously associated with cholesterol metabolism and apolipoprotein B measurements.[54]

Association of HBS1L-MYB and CPPED1 to the payoff steps of glycolysis (involving phosphoglycerate and phosphoenolpyruvate metabolism to pyruvate) and ATP suggests an association between energy metabolism and hemoglobin variants, including hemoglobin F[80] and alpha-thalassemia in the ATR-16 syndrome, deletions of ~177 to ~2000 kb affecting one allele of the well-characterized, gene dense, distal region of chromosome 16 (16p13.3) [81]. In the GWAS catalog CPPED1 was previously only associated to body height, while HBS1L was previously linked to a series of hematological parameters, including RBC count, hemoglobin concentration, L-arginine levels, and neutrophil or eosinophil counts.

One major limitation of the mQTL studies is that genetically conserved, non-polymorphic regions would not be highlighted. Since our studies are based on volunteers who are sufficiently healthy to donate blood, genetic polymorphisms that are either incompatible with life or associated with major hematological effects would not be captured by our analysis. As such, signals from rare polymorphisms would not be detected unless additionally diverse populations (e.g., non-healthy, non-blood donors) were also investigated. Nonetheless, we did detect signals for genes like G6PD, PKLR or ADA, all of which are associated with hematological conditions, suggesting that signatures for these genotypes are still detectable in the metabolome of RBCs from otherwise asymptomatic heterozygous carriers who donate blood.

In conclusion, our findings provide “real-world” clinical data on the potential use of ATP and hypoxanthine levels as markers of stored RBC hemolytic propensity, both in the bag and, most importantly, in vivo following transfusion.[82] To this end, we combined autologous PTR studies on an independent cohort and clinical data from thousands of transfusion recipients of units from REDS RBC Omics donors by interrogating a “vein-to-vein” database[83]. Accumulation of hypoxanthine also informs on both energy and redox status of stored RBCs, as ATP consumption and deamination are favored by BPG consumption and oxidant stress, factors that contribute to the

enzymatic activity of AMPD3[26,27]. Current gold standards of RBC storage quality, in bag hemolysis and PTR, are not routinely tested for all issued blood products, rather they are only measured during the process of securing FDA or European Council approval for newly developed stored blood products. Here we show that stored RBC ATP and hypoxanthine levels are not only relevant surrogates for these measures, but are also amenable to ultra-high-throughput screening at scale, and could potentially be implemented for all of the >100 million RBC units donated worldwide. Since RBC ATP levels are also essential regulators of oxygen kinetics[84], our results are a step forward towards identifying markers that can not only inform on the quality of the stored products but also, potentially, predict their efficacy upon transfusion.

STAR METHODS

Donor recruitment in the REDS RBC Omics study:

Index donors A total of 13,758 donors were enrolled in the Recipient Epidemiology and Donor evaluation Study (REDS) RBC Omics at four different blood centers across the United States (https://biolincc.nhlbi.nih.gov/studies/reds_iii/). Of these, 97% (13,403) provided informed consent and 13,029 were available for metabolomics analyses in this study – henceforth referred to as "index donors". A subset of these donors were evaluable for hemolysis parameters, including spontaneous (n=12,753) in ~42-day stored leukocyte-filtered packed RBCs derived from whole blood donations from this cohort [45]. Methods for the determination of FDA-standard spontaneous (storage) hemolysis test, osmotic hemolysis (pink test) and oxidative hemolysis upon challenge with AAPH have been extensively described elsewhere [85].

Storage hemolysis In details, after storage under routine blood bank conditions (1-6°C) for 39 to 42 days, the contents of each unit was transferred into a 15-mL conical tube from which 2 aliquots (1 mL each) were processed for the hemolytic assays. One aliquot was used for the quantification of spontaneous storage hemolysis and the other for the stress-induced hemolysis assays. Percent end-of-storage hemolysis was determined according to the following equation:

$$\textit{Storage hemolysis (\%)} = (100\text{-}HCT)\ Hb_{supernatant} : Hb_{total}$$

Sample hematocrit (HCT) was determined by collecting blood samples into capillary tubes, which were centrifuged in a micro-HCT centrifuge (LW Scientific, Lawrenceville, GA). $Hb_{supernatant}$ refers to the levels of free hemoglobin obtained after centrifugation (1500g, 10 minutes, 18°C) measured in the supernatant. Hb_{total} refers to the total amount of sample hemoglobin before centrifugation. In the entire study, hemoglobin concentrations (micromolar) were determined by Drabkin's method.[86]

For the evaluation of stress-induced hemolysis, stored RBCs were washed (1500g, 10 minutes, 18°C) 3 times with phosphate-buffered saline (PBS) to remove plasma and additive solution, and immediately subjected to osmotic or oxidative stress assays.

RBC osmotic hemolysis

Osmotic hemolysis was determined by a modified pink test assay previously used for diagnosis of genetic mutations that affect RBC osmotic fragility (eg, sickle cell disease, thalassemia, and spherocytosis) [87,88]. Washed RBCs were incubated under static conditions (4 hours at 22°C) in pink test buffer (a hypotonic Bis-Tris buffer containing 25 mmol/L sodium chloride, 70 mmol/L 2,2-Bis(hydroxymethyl)-2,2′,2″nitrilotriethanol (Bis-Tris) buffer, and 135 mmol/L glycerol; pH 6.6) at a

final concentration of 1.6% ± 0.2% after which samples were centrifuged (1500g, 10 minutes, 18°C), and percent osmotic hemolysis was determined:

$$Osmotic\ hemolysis\ (\%) = (Hb_{Osmotic} - Hb_{total}) \times 100$$

for which Hbosmotic corresponds to supernatant cell-free hemoglobin of pink test–treated RBCs, and Hb_{total} refers to the total amount of hemoglobin in each sample.

RBC oxidative hemolysis

Testing for donor differences in RBC susceptibility to oxidative hemolysis was performed as described by Kanias et al., [85] by incubating RBCs in the presence of 2,2′-azobis-2-methyl-propanimidamide dihydrochloride (AAPH; 150 mmoL). Thermal (37°C) decomposition of AAPH generates peroxyl radicals leading to lipid peroxidation–mediated hemolysis.24 Washed RBCs were suspended with PBS to a final concentration of 3.5% ± 0.5%. Aliquots (0.21 mL) were transferred into microplates to which 0.09 mL of AAPH (0.5 M) or PBS was added. The plates were incubated (37°C) under static conditions for 1.5 hours, after which the plates were centrifuged (1500g, 10 minutes, 18°C), and AAPH-induced oxidative hemolysis was determined by using the following formula:

$$Oxidative\ hemolysis\ (\%) = (Hb_{AAPH} - Hb_{control}) : Hb_{total} \times 100$$

where Hb_{AAPH} corresponds to supernatant cell-free hemoglobin of AAPH-treated RBCs, $Hb_{control}$ corresponds to supernatant cell-free hemoglobin from untreated RBCs, and Hb_{total} refers to the total amount of hemoglobin in each sample.

Recalled donors: A total of 643 donors scoring in the 5th and 95th percentile for hemolysis parameters at the index phase of the study were invited to donate a second unit of pRBCs, a cohort henceforth referred to as "recalled donors". These units were assayed at storage days 10, 23 and 42 for hemolytic parameters and mass spectrometry-based high-throughput metabolomics [89], proteomics [90], lipidomics [91] and ICP-MS analyses [92]. Under the aegis of the REDS-IV-P project [93], a total of 1,929 samples (n=643, storage day 10, 23 and 42) were processed with this multi-omics workflow. Extracellular vesicles were measured by flow-cytometry [94].

Donor iron deficiency study (DIDS) A total of 79 repeat blood donors were enrolled as part of the DIDS study for baseline and post-iron repletion before determination of autologous post-transfusion recovery (PTR) studies of day 42 stored units with ^{51}Cr, as described [65].

High-throughput metabolomics Metabolomics extraction and analyses in 96 well-plate format were performed as described.[95,96] RBC samples were transferred on ice on 96 well plate and frozen at -80 ºC at Vitalant San Francisco prior to shipment in dry ice to the University of Colorado

Anschutz Medical Campus. Plates were thawed on ice then a 10 uL aliquot was transferred with a multi-channel pipettor to 96-well extraction plates. A volume of 90 uL of ice cold 5:3:2 MeOH:MeCN:water (*v/v/v*) was added to each well, with an electronically-assisted cycle of sample mixing repeated three times. Extracts were transferred to 0.2 µm filter plates (Biotage) and insoluble material was removed under positive pressure using nitrogen applied via a 96-well plate manifold. Filtered extracts were transferred to an ultra-high-pressure liquid chromatography (UHPLC-MS — Vanquish) equipped with a plate charger. A blank containing a mix of standards detailed before[97] and a quality control sample (the same across all plates) were injected 2 or 4 times each per plate, respectively, to qualify instrument performance throughout the analysis. For each measured metabolite, median values on each plate were determined; all samples were normalized intra-plate to the respective median value prior to merging the entire dataset (principal component analyses – PCA of pre- vs post-normalization data are shown in **Supplementary Table 1**). Metabolites were resolved on a Phenomenex Kinetex C18 column (2.1 x 30 mm, 1.7 um) at 45 °C using a 1-minute ballistic gradient method in positive and negative ion modes (separate runs) over the scan range 65-975 m/z exactly as previously described [95]. The UHPLC was coupled online to a Q Exactive mass spectrometer (Thermo Fisher). The Q Exactive MS was operated in negative ion mode, scanning in Full MS mode (2 µscans) from 90 to 900 m/z at 70,000 resolution, with 4 kV spray voltage, 45 sheath gas, 15 auxiliary gas. Following data acquisition, .raw files were converted to .mzXML using RawConverter then metabolites assigned and peaks integrated using ElMaven (Elucidata) in conjunction with an in-house standard library [98]. A list of experimental m/z, retention times, metabolite IDs (either KEGG or HMDB) and adducts is provided in **supplementary table 1**.

High-throughput proteomics Proteomics analyses were performed as described.[50,99] A volume of 10 µL of RBCs were lysed in 90 µL of distilled water; 5 µL of lysed RBCs were mixed with 45 µL of 5% SDS and then vortexed. Samples were reduced with 10 mM DTT at 55 °C for 30 min, cooled to room temperature, and then alkylated with 25 mM iodoacetamide in the dark for 30 min. Next, a final concentration of 1.2% phosphoric acid and then six volumes of binding buffer (90% methanol; 100 mM triethylammonium bicarbonate, TEAB; pH 7.1) were added to each sample. After gentle mixing, the protein solution was loaded to a S-Trap 96-well plate, spun at 1500 x g for 2 min, and the flow-through collected and reloaded onto the 96-well plate. This step was repeated three times, and then the 96-well plate was washed with 200 µL of binding buffer 3 times. Finally, 1 µg of sequencing-grade trypsin (Promega) and 125 µL of digestion buffer (50 mM TEAB) were added onto the filter and digested carried out at 37 °C for 6 h. To elute peptides, three stepwise buffers were applied, with 100 µL of each with one more repeat, including 50 mM TEAB, 0.2% formic acid

(FA), and 50% acetonitrile and 0.2% FA. The peptide solutions were pooled, lyophilized, and resuspended in 500 μL of 0.1 % FA. Each sample was loaded onto individual Evotips for desalting and then washed with 200 μL 0.1% FA followed by the addition of 100 μL storage solvent (0.1% FA) to keep the Evotips wet until analysis. The Evosep One system (Evosep, Odense, Denmark) was used to separate peptides on a Pepsep column, (150 um inter diameter, 15 cm) packed with ReproSil C18 1.9 μm, 120A resin. The system was coupled to a timsTOF Pro mass spectrometer (Bruker Daltonics, Bremen, Germany) via a nano-electrospray ion source (Captive Spray, Bruker Daltonics). The mass spectrometer was operated in PASEF mode. The ramp time was set to 100 ms and 10 PASEF MS/MS scans per topN acquisition cycle were acquired. MS and MS/MS spectra were recorded from *m/z* 100 to 1700. The ion mobility was scanned from 0.7 to 1.50 Vs/cm2. Precursors for data-dependent acquisition were isolated within ± 1 Th and fragmented with an ion mobility-dependent collision energy, which was linearly increased from 20 to 59 eV in positive mode. Low-abundance precursor ions with an intensity above a threshold of 500 counts but below a target value of 20000 counts were repeatedly scheduled and otherwise dynamically excluded for 0.4 min.

Preparation of pure mature RBCs Whole blood was obtained from 6 healthy donor volunteers at Columbia University in New York, NY, USA, upon signing of informed consent. Whole blood from 5 healthy volunteers was collected into EDTA tubes. Blood was spun at 800g for 10 minutes, plasma was removed, and 50uL of packed RBCs from each donor was combined prior to leukoreduction via filtration (Pall Medical) to remove log4 (99.99%) and log2.5 residual white blood cells (WBCs) and platelets (PLTs), respectively, as standard workflow in modern blood banks in most US states.[100]. The mixed RBCs were washed in PBS and 200uL of packed RBCs was resuspended in 10mL PBS and stained with antibodies CD45 PE-Cy7 (1:400), CD41 APC-Cy7 (1:400), CD235a BV605 (1:1000), and CD71 PE (1:100) for 20 minutes at room temperature. Samples were washed with PBS and resuspended to a final volume of 1mL. Immediately before sorting, 30uL of RBCs was diluted into 10mL PBS supplemented with 20uL thiazole orange. Purified RBC populations were achieved using BD FACSAria cell sorters. CD45+ white blood cell and CD41+ platelets were excluded from RBC singlets and reticulocytes (CD235a+TO+) and mature RBCs (CD23a+CD71-TO-) were sorted. Aliquots of sorted cells were re-analyzed on the cell sorter to determine purity, indicating >99.99% mature RBCs.

mQTL analysis in REDS RBC Omics The workflow for the mQTL analysis of ATP, hypoxanthine and glycolytic metabolites is consistent with previously described methods from our

pilot mQTL study on 250 recalled donors.[101] Details of the genotyping and imputation of the RBC Omics study participants have been previously described by Page, et al. [31] and Nemkov et al. [50] Metabolites with missing data and zeros were both treated identically. We separated the participant data by blood storage additive type and excluded metabolites with greater than 10% missingness from each additive set, respectively. Relatively quantified metabolites were natural log transformed. These groups of metabolites then had missing metabolite levels imputed using QRILC[102], implemented in the R package QRILC[102]. After imputation, all metabolites were inverse normal transformed using the R package GenABEL rntransform command[103]. Metabolites with more than 10% missing were not considered in these analyses. Briefly, genotyping was performed using a Transfusion Medicine microarray [104] consisting of 879,000 single nucleotide polymorphisms (SNPs); the data are available in dbGAP accession number phs001955.v1.p1. Imputation was performed using 811,782 SNPs that passed quality control. After phasing using Shape-IT [105], imputation was performed using Impute2 [106] with the 1000 Genomes Project phase 3 [106] all-ancestry reference haplotypes. We used the R package SNPRelate [107] to calculate principal components (PCs) of ancestry. We performed association analyses for glycolytic metabolites using an additive SNP model in the R package ProbABEL [108] and 13,091 study participants who had both metabolomics data and imputation data on serial samples from stored RBC components that passed respective quality control procedures. We adjusted for sex, age (continuous), frequency of blood donation in the last two years (continuous), blood donor center, and ten ancestry PCs. Statistical significance was determined using a p-value threshold of $5x10^{-8}$. We only considered variants with a minimum minor allele frequency of 1% and a minimum imputation quality score of 0.80. The OASIS: Omics Analysis, Search & Information a TOPMED funded resources[109], was used to annotate the top SNPs. OASIS annotation includes information on position, chromosome, allele frequencies, closest gene, type of variant, position relative to closest gene model, if predicted to functionally consequential, tissues specific gene expression, and other information.

Mouse RBC storage and post-transfusion recovery Mouse storage and PTR studies were performed as previously described [110], leveraging a population of 525 Diversity Outbred mice obtained from the Jackson Laboratory (J:DO). J:DO mice were derived from extensive outbreeding of eight inbred founder strains that represent genetically distinct lineages of the house mouse [111]. All animal procedures were approved by the University of Virginia IACUC (protocol no. 4269). All animals were genotyped at 143,259 SNPs (137,192 loci after filtering) using the GigaMUGA array [112].

mQTL analysis in JAX DO mice The mQTL workflow in JAX DO mice followed previously defined conventions [113]. Briefly, metabolite values of zero were converted to a missing value and only metabolites with 100 non-missing observations or more were included for further analyses. Each metabolite was transformed to normal quantiles for mQTL analysis to reduce the influence of outlying values. The initial mQTL mapping was based on founder strain haplotypes imputed at SNPs (137,192 loci), allowing for the additive genetic effects at loci to be more richly characterized as eight founder allele effects. Sex (43% females and 57% males) and sub-cohorts (5 groups/batches) were adjusted for as covariates. A lenient significance threshold of LOD score > 6 was used for calling mQTL to allow for the detection of mQTL hot spots. For reference, a LOD score > 8 approximately represents a genome-wide adjusted p-value < 0.05 [114]. Fine mapping at detected mQTL was performed by imputing variants based on the genotypes of the founder strains (GRCm39). We used the same mQTL workflow for fresh and stored RBCs. All analyses were performed using the R package qtl2 [113]. Processed data and results are uploaded to the QTLViewer webtool (https://churchilllab.jax.org/qtlviewer/Zimring/RBC;[115]) for interactive analyses and download. All data and code for the analysis pipeline are available at figshare (https://doi.org/10.6084/m9.figshare.24456619).

Dynamic modeling of PFKP

To understand the role of the PFKP isozyme in human RBCs, we used the MASSpy python package to reconstruct a mass action stoichiometric simulation model of the in vivo RBC glycolytic pathway at steady state[55,56]. First, we replaced mass action rate laws with detailed enzyme kinetic equations and parameters for key regulatory enzymes hexokinase, phosphofructokinase, and pyruvate kinase[59,60]. Then, we assumed that the existing PFK reaction was catalyzed by the tetrameric enzyme formed by liver and muscle isozymes in erythrocytes. Mature RBCs do not contain significant concentrations of fructose 2,6-bisphosphate; therefore we assumed that fructose 2,6-bisphosphate is negligible as an effector in the intracellular RBC environment. We then created a second copy of the model and modified it with a second PFK reaction to represent the platelet isozyme, whose concentration estimates as a fraction of total PFK isoforms were based on proteomics measurements in the present study. We parameterized the PFKP isozyme in the model relative to the PFKL isozyme from true comparative and protein structure studies where possible to avoid discrepancies due to different assay conditions across studies[57,62-64]. Models representing RBC glycolysis with PFKP and without PFKP were simulated after a sudden 80% decrease in ATP concentration.

Determination of hemoglobin and bilirubin increment via the vein-to-vein database Association of metabolite levels with hemoglobin and bilirubin increment was performed by interrogating the vein-to-vein database, as described in Roubinian et al. [32,83] Bucketing of metabolite levels in quartiles and tertiles for hemoglobin and bilirubin increments was informed by the significantly smaller record of entries for the latter parameter in the database.

Vein-to-vein database: General Study Design We conducted a retrospective cohort study using electronic health records from the National Heart Lung and Blood Institute (NHLBI) Recipient Epidemiology and Donor Evaluation Study-III (REDS-III) program available as public use data through BioLINCC [116,117]. The database includes blood donor, component manufacturing, and patient data collected at 12 academic and community hospitals from four geographically diverse regions in the United States (Connecticut, Pennsylvania, Wisconsin, and California) for the 4-year period from January 1, 2013 to December 31, 2016. Genotype and metabolomic data from the subset of blood donors who participated in the REDS-III RBC-Omics study [118] was linked to the dataset using unique donor identifiers.

Study Population and Definitions Data regarding blood donor demographics (e.g., age, sex, body mass index, ABO/Rh), collection date and methods (e.g., whole blood or apheresis), as well as component manufacturing characteristics (e.g., timing of leukoreduction, additive solution, irradiation status) were extracted for each RBC unit collected. Available donor genetic polymorphism and metabolomic data was linked to issued RBC units using random donor identification numbers. Among transfusion recipients, we included all adult patients who received a single RBC unit during one or more transfusion episodes between January 1, 2013 and December 30, 2016. Recipient details included age, sex, body mass index (BMI), along with storage age, and blood product issue date and time. We collected hemoglobin and bilirubin levels measured by the corresponding clinical laboratory prior to and following each RBC transfusion event.

Transfusion Exposures and Outcome Measures All single RBC unit transfusion episodes linked to genetic polymorphism and metabolomic data were included in this analysis. A RBC unit transfusion episode was defined as any single RBC transfusion from a single donor with both informative pre- and post-transfusion laboratory measures and without any other RBC units transfused in the following 24-hour time period. The outcome measures of interest were change in hemoglobin (ΔHb; g/dL) and change in total bilirubin (ΔBi; mg/dL) following a single RBC unit transfusion episode. These measurements were adjusted for all of the other co-factors - including

donor age, sex, hemoglobin - component apheresis, irradiation, storage age, storage solution, recipient age, sex, body mass index, and hemoglobin level. These outcomes were defined as the difference between the post-transfusion and pre-transfusion levels. Pre-transfusion thresholds for these measures were chosen to limit patient confounding (e.g., underlying hepatic disease). For pre-transfusion hemoglobin, the value used was the most proximal hemoglobin measurements prior to RBC transfusion, but at most 24 hours prior to transfusion. Furthermore, we excluded transfusion episodes where the pre-transfusion hemoglobin was greater than 9.5 g/dL, and the hemoglobin increment may be confounded by hemorrhage events. For post-transfusion hemoglobin, the laboratory measure nearest to 24-hours post-transfusion, but between 12- and 36-hours following transfusion was used. For pre-transfusion bilirubin, the most proximal total bilirubin measurement prior to transfusion, but at most 7-days prior to transfusion was used. Furthermore, the pre-transfusion bilirubin had to be below 1.5 mg/dL for the transfusion to be considered to exclude patients with pre-existing liver disease. For post-transfusion bilirubin, the most proximal laboratory measure to the transfusion, but at most 24-hours post-transfusion was used.

Statistical Methods We assessed the univariable association of all *a priori* selected donor, manufacturing, and recipient covariates with the outcomes using linear regression. Multivariable linear regression assessed associations between alleles of donor single nucleotide polymorphisms and changes in hemoglobin and bilirubin levels post-transfusion hemoglobin. Two-sided p-values less than 0.05 were considered to be statistically significant. Analyses were performed using Stata Version 14.1, StataCorp, College Station, TX.

Data analysis Statistical analyses – including hierarchical clustering analysis (HCA), linear discriminant analysis (LDA), uniform Manifold Approximation and Projection (uMAP), correlation analyses and Lasso regression were performed using both MetaboAnalyst 5.0 [119] and in-house developed code in R (4.2.3 2023-03-15). Figures were generated in R, Python, MetaboAnalyst, Biorender (www.biorender.com).

Acknowledgements This study was supported by funds by the National Heart, Lung, and Blood Institute R21HL150032, R01HL146442, R01HL149714 (to AD and JCZ), R01HL148151 (to AD, SLS and JCZ) and R01HL126130 (NR). The authors acknowledge support from the REDS RBC Omics and REDS-IV-P CTLS programs, sponsored by the National Heart, Lung, and Blood Institute contract 75N2019D00033, and from the NHLBI Recipient Epidemiology and Donor Evaluation Study-III (REDS-III) RBC Omics project, which was supported by NHLBI contracts HHSN2682011-00001I, -00002I, -00003I, -00004I, -00005I, -00006I, -00007I, -00008I, and -00009I. The autologous post-transfusion recovery studies were funded by NHLBI R01HL133049. The content is solely the responsibility of the authors and does not necessarily represent the official views of the National Institutes of Health.

Authors' contributions TN, DS, AD performed metabolomics analyses. TN, DS, AD performed method development, quality control and metabolomics data analysis. EE, AM, GPP performed human mQTL analyses; GRK, GAC performed mQTL analyses for the Diversity Outbred mice; AH, JCZ performed the Diversity Outbred mouse studies; MD, KCH performed proteomics studies; ZH and BOP generated the metabolic reconstruction models; SLS, EAH performed post-transfusion recovery studies (DIDS cohort); CE, AK, XD, EE, GRK, GAC, NR, AD performed statistical analyses; NR performed linkage analyses to the vein-to-vein database; MS, PJN, SK, MPB performed and supervised the REDS RBC Omics study; TN, EE, GRK, AK, CE, AD prepared figure panels; AD wrote the first version of the manuscript, that was critically reviewed and approved by all authors.

Competing Interests The authors declare that AD, KCH, TN are founders of Omix Technologies Inc and Altis Biosciences LLC. AD, SLS and TN are Scientific Advisory Board (SAB) members for Hemanext Inc. AD is SAB member for Macopharma Inc. SLS is SAB member for Alcor, Inc and consultant for Tioma, Inc and Team Conveyer Intellectual Properties. SLS is also executive director for Worldwide Initiative for Rh Disease Eradication (WIRhE) and CEO for Ferrous Wheel Consultants, LLC. JCZ is a founder of Svalinn Therapeutics. All the other authors have no conflicts to disclose in relation to this study.

REFERENCES *(including STAR METHODS)*

1. Bianconi, E., Piovesan, A., Facchin, F., Beraudi, A., Casadei, R., Frabetti, F., Vitale, L., Pelleri, M.C., Tassani, S., Piva, F., et al. (2013). An estimation of the number of cells in the human body. Ann Hum Biol *40*, 463-471. 10.3109/03014460.2013.807878.
2. Kaestner, L., and Minetti, G. (2017). The potential of erythrocytes as cellular aging models. Cell Death Differ *24*, 1475-1477. 10.1038/cdd.2017.100.
3. D'Alessandro, A., Anastasiadi, A.T., Tzounakas, V.L., Nemkov, T., Reisz, J.A., Kriebardis, A.G., Zimring, J.C., Spitalnik, S.L., and Busch, M.P. (2023). Red Blood Cell Metabolism In Vivo and In Vitro. Metabolites *13*, 793.
4. Bardyn, M., Crettaz, D., Rappaz, B., Hamelin, R., Armand, F., Tissot, J.D., Turcatti, G., and Prudent, M. (2023). Phosphoproteomics and Morphology of Stored Human Red Blood Cells Treated by Protein-Tyrosine-Phosphatases Inhibitor. Blood Adv. 10.1182/bloodadvances.2023009964.
5. Xu, P., Chen, C., Zhang, Y., Dzieciatkowska, M., Brown, B.C., Zhang, W., Xie, T., Abdulmalik, O., Song, A., Tong, C., et al. (2022). Erythrocyte transglutaminase-2 combats hypoxia and chronic kidney disease by promoting oxygen delivery and carnitine homeostasis. Cell Metab *34*, 299-316.e296. 10.1016/j.cmet.2021.12.019.
6. Betz, T., Lenz, M., Joanny, J.-F., and Sykes, C. (2009). ATP-dependent mechanics of red blood cells. Proceedings of the National Academy of Sciences *106*, 15320-15325. doi:10.1073/pnas.0904614106.
7. Gokhin, D.S., and Fowler, V.M. (2016). Feisty filaments: actin dynamics in the red blood cell membrane skeleton. Curr Opin Hematol *23*, 206-214. 10.1097/moh.0000000000000227.
8. Wagner, G.M., Chiu, D.T., Yee, M.C., and Lubin, B.H. (1986). Red cell vesiculation--a common membrane physiologic event. J Lab Clin Med *108*, 315-324.
9. Arashiki, N., Takakuwa, Y., Mohandas, N., Hale, J., Yoshida, K., Ogura, H., Utsugisawa, T., Ohga, S., Miyano, S., Ogawa, S., et al. (2016). ATP11C is a major flippase in human erythrocytes and its defect causes congenital hemolytic anemia. Haematologica *101*, 559-565. 10.3324/haematol.2016.142273.
10. Tzounakas, V.L., Dzieciatkowska, M., Anastasiadi, A.T., Karadimas, D.G., Vergaki, A., Siourounis, P., Stamoulis, K., Papassideri, I.S., Kriebardis, A.G., D'Alessandro, A., and Antonelou, M.H. (2022). Red cell proteasome modulation by storage, redox metabolism and transfusion. Blood Transfus *20*, 27-39. 10.2450/2020.0179-20.
11. van Wijk, R., and van Solinge, W.W. (2005). The energy-less red blood cell is lost: erythrocyte enzyme abnormalities of glycolysis. Blood *106*, 4034-4042. 10.1182/blood-2005-04-1622.
12. D'Alessandro, A., Anastasiadi, A.T., Tzounakas, V.L., Nemkov, T., Reisz, J.A., Kriebardis, A.G., Zimring, J.C., Spitalnik, S.L., and Busch, M.P. (2023). Red Blood Cell Metabolism In Vivo and In Vitro. Metabolites *13*. 10.3390/metabo13070793.
13. Ahmed, M.H., Ghatge, M.S., and Safo, M.K. (2020). Hemoglobin: Structure, Function and Allostery. Subcell Biochem *94*, 345-382. 10.1007/978-3-030-41769-7_14.
14. Nemkov, T., Reisz, J.A., Xia, Y., Zimring, J.C., and D'Alessandro, A. (2018). Red blood cells as an organ? How deep omics characterization of the most abundant cell in the human body highlights other systemic metabolic functions beyond oxygen transport. Expert review of proteomics *15*, 855-864. 10.1080/14789450.2018.1531710.
15. Wiback, S.J., and Palsson, B.O. (2002). Extreme pathway analysis of human red blood cell metabolism. Biophys J *83*, 808-818. 10.1016/s0006-3495(02)75210-7.
16. Grüning, N.-M., and Ralser, M. (2021). Glycolysis: How a 300yr long research journey that started with the desire to improve alcoholic beverages kept revolutionizing biochemistry. Current Opinion in Systems Biology *28*, 100380. https://doi.org/10.1016/j.coisb.2021.100380.
17. Meyerhof, O., and Junowicz-Kocholaty, R. (1943). THE EQUILIBRIA OF ISOMERASE AND ALDOLASE, AND THE PROBLEM OF THE PHOSPHORYLATION OF GLYCERALDEHYDE PHOSPHATE. Journal of Biological Chemistry *149*, 71-92. https://doi.org/10.1016/S0021-9258(18)72218-7.

18. Tanner, L.B., Goglia, A.G., Wei, M.H., Sehgal, T., Parsons, L.R., Park, J.O., White, E., Toettcher, J.E., and Rabinowitz, J.D. (2018). Four Key Steps Control Glycolytic Flux in Mammalian Cells. Cell Syst *7*, 49-62.e48. 10.1016/j.cels.2018.06.003.
19. Custer, B., Bloch, E.M., Bryant, B.J., D'Alessandro, A., Delaney, M., Goel, R., Hod, E.A., Josephson, C.D., Katz, L.M., Miller, Y.M., et al. (2023). Proceedings of the 2022 NHLBI and OASH state of the science in transfusion medicine symposium. Transfusion *63*, 1074-1091. 10.1111/trf.17296.
20. Yoshida, T., Prudent, M., and D'Alessandro, A. (2019). Red blood cell storage lesion: causes and potential clinical consequences. Blood Transfus *17*, 27-52. 10.2450/2019.0217-18.
21. Sparrow, R.L. (2012). Time to revisit red blood cell additive solutions and storage conditions: a role for "omics" analyses. Blood Transfus *10 Suppl 2*, s7-11. 10.2450/2012.003s.
22. D'Alessandro, A., Nemkov, T., Yoshida, T., Bordbar, A., Palsson, B.O., and Hansen, K.C. (2017). Citrate metabolism in red blood cells stored in additive solution-3. Transfusion *57*, 325-336. 10.1111/trf.13892.
23. D'Alessandro, A., D'Amici, G.M., Vaglio, S., and Zolla, L. (2012). Time-course investigation of SAGM-stored leukocyte-filtered red bood cell concentrates: from metabolism to proteomics. Haematologica *97*, 107-115. 10.3324/haematol.2011.051789.
24. Hess, J.R., and D'Alessandro, A. (2022). Red blood cell metabolism and preservation. In Rossi's Principles of Transfusion Medicine, pp. 143-157. https://doi.org/10.1002/9781119719809.ch14.
25. Yurkovich, J.T., Zielinski, D.C., Yang, L., Paglia, G., Rolfsson, O., Sigurjónsson Ó, E., Broddrick, J.T., Bordbar, A., Wichuk, K., Brynjólfsson, S., et al. (2017). Quantitative time-course metabolomics in human red blood cells reveal the temperature dependence of human metabolic networks. J Biol Chem *292*, 19556-19564. 10.1074/jbc.M117.804914.
26. Nemkov, T., Sun, K., Reisz, J.A., Song, A., Yoshida, T., Dunham, A., Wither, M.J., Francis, R.O., Roach, R.C., Dzieciatkowska, M., et al. (2018). Hypoxia modulates the purine salvage pathway and decreases red blood cell and supernatant levels of hypoxanthine during refrigerated storage. Haematologica *103*, 361-372. 10.3324/haematol.2017.178608.
27. Chen, C., Xie, T., Zhang, Y., Wang, Y., Yu, F., Lin, L., Zhang, W., Brown, B.C., Zhang, X., Kellems, R.E., et al. (2023). Erythrocyte ENT1-AMPD3 Axis is an Essential Purinergic Hypoxia Sensor and Energy Regulator Combating CKD in a Mouse Model. J Am Soc Nephrol *34*, 1647-1671. 10.1681/asn.0000000000000195.
28. Paglia, G., D'Alessandro, A., Rolfsson, O., Sigurjonsson, O.E., Bordbar, A., Palsson, S., Nemkov, T., Hansen, K.C., Gudmundsson, S., and Palsson, B.O. (2016). Biomarkers defining the metabolic age of red blood cells during cold storage. Blood *128*, e43-50. 10.1182/blood-2016-06-721688.
29. Rolfsson, Ó., Sigurjonsson Ó, E., Magnusdottir, M., Johannsson, F., Paglia, G., Guðmundsson, S., Bordbar, A., Palsson, S., Brynjólfsson, S., Guðmundsson, S., and Palsson, B. (2017). Metabolomics comparison of red cells stored in four additive solutions reveals differences in citrate anticoagulant permeability and metabolism. Vox Sang *112*, 326-335. 10.1111/vox.12506.
30. Isiksacan, Z., D'Alessandro, A., Wolf, S.M., McKenna, D.H., Tessier, S.N., Kucukal, E., Gokaltun, A.A., William, N., Sandlin, R.D., Bischof, J., et al. (2023). Assessment of stored red blood cells through lab-on-a-chip technologies for precision transfusion medicine. Proceedings of the National Academy of Sciences *120*, e2115616120. doi:10.1073/pnas.2115616120.
31. Page, G.P., Kanias, T., Guo, Y.J., Lanteri, M.C., Zhang, X., Mast, A.E., Cable, R.G., Spencer, B.R., Kiss, J.E., Fang, F., et al. (2021). Multiple-ancestry genome-wide association study identifies 27 loci associated with measures of hemolysis following blood storage. J Clin Invest *131*. 10.1172/jci146077.
32. Roubinian, N.H., Reese, S.E., Qiao, H., Plimier, C., Fang, F., Page, G.P., Cable, R.G., Custer, B., Gladwin, M.T., Goel, R., et al. (2022). Donor genetic and nongenetic factors affecting red blood cell transfusion effectiveness. JCI Insight *7*. 10.1172/jci.insight.152598.
33. Francis, R.O., Mahajan, S., Rapido, F., La Carpia, F., Soffing, M., Divgi, C., Yeh, R., Mintz, A., Leslie, L., Agrest, I., et al. (2019). Reexamination of the chromium-51-labeled posttransfusion red blood cell recovery method. Transfusion *59*, 2264-2275. 10.1111/trf.15310.

34. Van 't Erve, T.J., Wagner, B.A., Martin, S.M., Knudson, C.M., Blendowski, R., Keaton, M., Holt, T., Hess, J.R., Buettner, G.R., Ryckman, K.K., et al. (2015). The heritability of hemolysis in stored human red blood cells. Transfusion *55*, 1178-1185. 10.1111/trf.12992.
35. Lanteri, M.C., Kanias, T., Keating, S., Stone, M., Guo, Y., Page, G.P., Brambilla, D.J., Endres-Dighe, S.M., Mast, A.E., Bialkowski, W., et al. (2019). Intradonor reproducibility and changes in hemolytic variables during red blood cell storage: results of recall phase of the REDS-III RBC-Omics study. Transfusion *59*, 79-88. https://doi.org/10.1111/trf.14987.
36. Dumont, L.J., and AuBuchon, J.P. (2008). Evaluation of proposed FDA criteria for the evaluation of radiolabeled red cell recovery trials. Transfusion *48*, 1053-1060. 10.1111/j.1537-2995.2008.01642.x.
37. Custer, B., Bloch, E.M., Bryant, B.J., D'Alessandro, A., Delaney, M., Goel, R., Hod, E.A., Josephson, C.D., Katz, L.M., Miller, Y.M., et al. Proceedings of the 2022 NHLBI and OASH state of the science in transfusion medicine symposium. Transfusion *n/a*. https://doi.org/10.1111/trf.17296.
38. Vostal, J.G., Buehler, P.W., Gelderman, M.P., Alayash, A.I., Doctor, A., Zimring, J.C., Glynn, S.A., Hess, J.R., Klein, H., Acker, J.P., et al. (2018). Proceedings of the Food and Drug Administration's public workshop on new red blood cell product regulatory science 2016. Transfusion *58*, 255-266. 10.1111/trf.14435.
39. Surendran, P., Stewart, I.D., Au Yeung, V.P.W., Pietzner, M., Raffler, J., Wörheide, M.A., Li, C., Smith, R.F., Wittemans, L.B.L., Bomba, L., et al. (2022). Rare and common genetic determinants of metabolic individuality and their effects on human health. Nature Medicine *28*, 2321-2332. 10.1038/s41591-022-02046-0.
40. Childs, B. (1970). Sir Archibald Garrod's Conception of Chemical Individuality: A Modern Appreciation. New England Journal of Medicine *282*, 71-77. 10.1056/nejm197001082820205.
41. Draisma, H.H.M., Pool, R., Kobl, M., Jansen, R., Petersen, A.-K., Vaarhorst, A.A.M., Yet, I., Haller, T., Demirkan, A., Esko, T., et al. (2015). Genome-wide association study identifies novel genetic variants contributing to variation in blood metabolite levels. Nature Communications *6*, 7208. 10.1038/ncomms8208.
42. Van Dooijeweert, B., Broeks, M.H., Verhoeven-Duif, N.M., Van Beers, E.J., Nieuwenhuis, E.E.S., Van Solinge, W.W., Bartels, M., Jans, J.J., and Van Wijk, R. (2021). Untargeted metabolic profiling in dried blood spots identifies disease fingerprint for pyruvate kinase deficiency. Haematologica *106*, 2720-2725. 10.3324/haematol.2020.266957.
43. Francis, R.O., D'Alessandro, A., Eisenberger, A., Soffing, M., Yeh, R., Coronel, E., Sheikh, A., Rapido, F., La Carpia, F., Reisz, J.A., et al. (2020). Donor glucose-6-phosphate dehydrogenase deficiency decreases blood quality for transfusion. J Clin Invest *130*, 2270-2285. 10.1172/JCI133530.
44. Appiah, D., Nwabuo, C.C., Ebong, I.A., Wellons, M.F., and Winters, S.J. (2021). Trends in Age at Natural Menopause and Reproductive Life Span Among US Women, 1959-2018. JAMA *325*, 1328-1330. 10.1001/jama.2021.0278.
45. D'Alessandro, A., Culp-Hill, R., Reisz, J.A., Anderson, M., Fu, X., Nemkov, T., Gehrke, S., Zheng, C., Kanias, T., Guo, Y., et al. (2019). Heterogeneity of blood processing and storage additives in different centers impacts stored red blood cell metabolism as much as storage time: lessons from REDS-III-Omics. Transfusion *59*, 89-100. 10.1111/trf.14979.
46. D'Alessandro, A., Nemkov, T., Hansen, K.C., Szczepiorkowski, Z.M., and Dumont, L.J. (2015). Red blood cell storage in additive solution-7 preserves energy and redox metabolism: a metabolomics approach. Transfusion *55*, 2955-2966. 10.1111/trf.13253.
47. D'Alessandro, A., Nemkov, T., Kelher, M., West, F.B., Schwindt, R.K., Banerjee, A., Moore, E.E., Silliman, C.C., and Hansen, K.C. (2015). Routine storage of red blood cell (RBC) units in additive solution-3: a comprehensive investigation of the RBC metabolome. Transfusion *55*, 1155-1168. 10.1111/trf.12975.
48. D'Alessandro, A., Reisz, J.A., Culp-Hill, R., Korsten, H., van Bruggen, R., and de Korte, D. (2018). Metabolic effect of alkaline additives and guanosine/gluconate in storage solutions for red blood cells. Transfusion *58*, 1992-2002. 10.1111/trf.14620.

49. Bordbar, A., Johansson, P.I., Paglia, G., Harrison, S.J., Wichuk, K., Magnusdottir, M., Valgeirsdottir, S., Gybel-Brask, M., Ostrowski, S.R., Palsson, S., et al. (2016). Identified metabolic signature for assessing red blood cell unit quality is associated with endothelial damage markers and clinical outcomes. Transfusion *56*, 852-862. 10.1111/trf.13460.
50. Nemkov, T., Stephenson, D., Erickson, C., Dzieciatkowska, M., Key, A., Moore, A., Earley, E.J., Page, G.P., Lacroix, I.S., Stone, M., et al. (2023). Regulation of kynurenine metabolism by blood donor genetics and biology impacts red cell hemolysis in vitro and in vivo. Blood. 10.1182/blood.2023022052.
51. Howie, H.L., Hay, A.M., de Wolski, K., Waterman, H., Lebedev, J., Fu, X., Culp-Hill, R., D'Alessandro, A., Gorham, J.D., Ranson, M.S., et al. (2019). Differences in Steap3 expression are a mechanism of genetic variation of RBC storage and oxidative damage in mice. Blood Advances *3*, 2272-2285. 10.1182/bloodadvances.2019000605.
52. Ceroni, F., Sagar, A., Simpson, N.H., Gawthrope, A.J., Newbury, D.F., Pinto, D., Francis, S.M., Tessman, D.C., Cook, E.H., Monaco, A.P., et al. (2014). A deletion involving CD38 and BST1 results in a fusion transcript in a patient with autism and asthma. Autism Res *7*, 254-263. 10.1002/aur.1365.
53. Quarona, V., Zaccarello, G., Chillemi, A., Brunetti, E., Singh, V.K., Ferrero, E., Funaro, A., Horenstein, A.L., and Malavasi, F. (2013). CD38 and CD157: a long journey from activation markers to multifunctional molecules. Cytometry B Clin Cytom *84*, 207-217. 10.1002/cyto.b.21092.
54. Sollis, E., Mosaku, A., Abid, A., Buniello, A., Cerezo, M., Gil, L., Groza, T., Güneş, O., Hall, P., Hayhurst, J., et al. (2022). The NHGRI-EBI GWAS Catalog: knowledgebase and deposition resource. Nucleic Acids Research *51*, D977-D985. 10.1093/nar/gkac1010.
55. Haiman, Z.B., Zielinski, D.C., Koike, Y., Yurkovich, J.T., and Palsson, B.O. (2021). MASSpy: Building, simulating, and visualizing dynamic biological models in Python using mass action kinetics. PLoS Comput Biol *17*, e1008208. 10.1371/journal.pcbi.1008208.
56. Jamshidi, N., and Palsson, B. (2010). Mass action stoichiometric simulation models: incorporating kinetics and regulation into stoichiometric models. Biophys J *98*, 175-185. 10.1016/j.bpj.2009.09.064.
57. Fernandes, P.M., Kinkead, J., McNae, I., Michels, P.A.M., and Walkinshaw, M.D. (2020). Biochemical and transcript level differences between the three human phosphofructokinases show optimisation of each isoform for specific metabolic niches. Biochem J *477*, 4425-4441. 10.1042/bcj20200656.
58. Mulukutla, B.C., Yongky, A., Daoutidis, P., and Hu, W.S. (2014). Bistability in glycolysis pathway as a physiological switch in energy metabolism. PLoS One *9*, e98756. 10.1371/journal.pone.0098756.
59. Mulquiney, P.J., and Kuchel, P.W. (1999). Model of 2,3-bisphosphoglycerate metabolism in the human erythrocyte based on detailed enzyme kinetic equations: equations and parameter refinement. Biochem J *342 Pt 3*, 581-596.
60. Nishino, T., Yachie-Kinoshita, A., Hirayama, A., Soga, T., Suematsu, M., and Tomita, M. (2013). Dynamic simulation and metabolome analysis of long-term erythrocyte storage in adenine-guanosine solution. PLoS One *8*, e71060. 10.1371/journal.pone.0071060.
61. Meienhofer, M.C., Lagrange, J.L., Cottreau, D., Lenoir, G., Dreyfus, J.C., and Kahn, A. (1979). Phosphofructokinase in human blood cells. Blood *54*, 389-400.
62. Dunaway, G.A., Kasten, T.P., Sebo, T., and Trapp, R. (1988). Analysis of the phosphofructokinase subunits and isoenzymes in human tissues. Biochem J *251*, 677-683. 10.1042/bj2510677.
63. Kloos, M., Brüser, A., Kirchberger, J., Schöneberg, T., and Sträter, N. (2015). Crystal structure of human platelet phosphofructokinase-1 locked in an activated conformation. Biochem J *469*, 421-432. 10.1042/bj20150251.
64. Meienhofer, M.C., Cottreau, D., Dreyfus, J.C., and Kahn, A. (1980). Kinetic properties of human F4 phosphofructokinase: a poor regulatory enzyme. FEBS Lett *110*, 219-222. 10.1016/0014-5793(80)80077-9.
65. Hod, E.A., Brittenham, G.M., Bitan, Z.C., Feit, Y., Gaelen, J.I., La Carpia, F., Sandoval, L.A., Zhou, A.T., Soffing, M., Mintz, A., et al. (2022). A randomized trial of blood donor iron repletion on red cell

quality for transfusion and donor cognition and well-being. Blood *140*, 2730-2739. 10.1182/blood.2022017288.
66. Nemkov, T., Sun, K., Reisz, J.A., Yoshida, T., Dunham, A., Wen, E.Y., Wen, A.Q., Roach, R.C., Hansen, K.C., Xia, Y., and D'Alessandro, A. (2017). Metabolism of Citrate and Other Carboxylic Acids in Erythrocytes As a Function of Oxygen Saturation and Refrigerated Storage. Front Med (Lausanne) *4*, 175. 10.3389/fmed.2017.00175.
67. Bordbar, A., Yurkovich, J.T., Paglia, G., Rolfsson, O., Sigurjónsson, Ó.E., and Palsson, B.O. (2017). Elucidating dynamic metabolic physiology through network integration of quantitative time-course metabolomics. Scientific Reports *7*, 46249. 10.1038/srep46249.
68. Simpson, R.J., Brindle, K.M., and Campbell, I.D. (1982). Spin ECHO proton NMR studies of the metabolism of malate and fumarate in human erythrocytes. Dependence on free NAD levels. Biochim Biophys Acta *721*, 191-200. 10.1016/0167-4889(82)90068-4.
69. Hue, L., and Taegtmeyer, H. (2009). The Randle cycle revisited: a new head for an old hat. Am J Physiol Endocrinol Metab *297*, E578-591. 10.1152/ajpendo.00093.2009.
70. Costello, L.C., and Franklin, R.B. (2016). Plasma Citrate Homeostasis: How It Is Regulated; And Its Physiological and Clinical Implications. An Important, But Neglected, Relationship in Medicine. HSOA J Hum Endocrinol *1*.
71. Williams, N.C., and O'Neill, L.A.J. (2018). A Role for the Krebs Cycle Intermediate Citrate in Metabolic Reprogramming in Innate Immunity and Inflammation. Frontiers in Immunology *9*. 10.3389/fimmu.2018.00141.
72. Icard, P., Coquerel, A., Wu, Z., Gligorov, J., Fuks, D., Fournel, L., Lincet, H., and Simula, L. (2021). Understanding the Central Role of Citrate in the Metabolism of Cancer Cells and Tumors: An Update. Int J Mol Sci *22*. 10.3390/ijms22126587.
73. Lee, H.C., Deng, Q.W., and Zhao, Y.J. (2022). The calcium signaling enzyme CD38 - a paradigm for membrane topology defining distinct protein functions. Cell Calcium *101*, 102514. https://doi.org/10.1016/j.ceca.2021.102514.
74. De Flora, A., Zocchi, E., Guida, L., Franco, L., and Bruzzone, S. (2004). Autocrine and paracrine calcium signaling by the CD38/NAD+/cyclic ADP-ribose system. Ann N Y Acad Sci *1028*, 176-191. 10.1196/annals.1322.021.
75. Sanghvi, V.R., Leibold, J., Mina, M., Mohan, P., Berishaj, M., Li, Z., Miele, M.M., Lailler, N., Zhao, C., de Stanchina, E., et al. (2019). The Oncogenic Action of NRF2 Depends on De-glycation by Fructosamine-3-Kinase. Cell *178*, 807-819.e821. 10.1016/j.cell.2019.07.031.
76. Mosca, L., Penco, S., Patrosso, M.C., Marocchi, A., Lapolla, A., Sartore, G., Chilelli, N.C., Paleari, R., and Mosca, A. (2011). Genetic variability of the fructosamine 3-kinase gene in diabetic patients. Clin Chem Lab Med *49*, 803-808. 10.1515/cclm.2011.133.
77. Delobel, J., Prudent, M., Rubin, O., Crettaz, D., Tissot, J.D., and Lion, N. (2012). Subcellular fractionation of stored red blood cells reveals a compartment-based protein carbonylation evolution. J Proteomics *76 Spec No.*, 181-193. 10.1016/j.jprot.2012.05.004.
78. D'Alessandro, A., Mirasole, C., and Zolla, L. (2013). Haemoglobin glycation (Hb1Ac) increases during red blood cell storage: a MALDI-TOF mass-spectrometry-based investigation. Vox Sang *105*, 177-180. 10.1111/vox.12029.
79. D'Alessandro, A., Earley, E.J., Nemkov, T., Stephenson, D., Dzieciatkowska, M., Hansen, K.C., Minetti, G., Champigneulle, B., Stauffer, E., Pichon, A., et al. (2024). Genetic polymorphisms and expression of Rhesus blood group RHCE are associated with 2,3-bisphosphoglycerate in humans at high altitude. Proc Natl Acad Sci U S A *121*, e2315930120. 10.1073/pnas.2315930120.
80. El-Ghamrawy, M., Yassa, M.E., Tousson, A.M.S., El-Hady, M.A., Mikhaeil, E., Mohamed, N.B., and Khorshied, M.M. (2020). Association between BCL11A, HSB1L-MYB, and XmnI γG-158 (C/T) gene polymorphism and hemoglobin F level in Egyptian sickle cell disease patients. Ann Hematol *99*, 2279-2288. 10.1007/s00277-020-04187-z.

81. Babbs, C., Brown, J., Horsley, S.W., Slater, J., Maifoshie, E., Kumar, S., Ooijevaar, P., Kriek, M., Dixon-McIver, A., Harteveld, C.L., et al. (2020). ATR-16 syndrome: mechanisms linking monosomy to phenotype. J Med Genet *57*, 414-421. 10.1136/jmedgenet-2019-106528.
82. Heaton, W.A., Keegan, T., Holme, S., and Momoda, G. (1989). Evaluation of 99mtechnetium/51chromium post-transfusion recovery of red cells stored in saline, adenine, glucose, mannitol for 42 days. Vox Sang *57*, 37-42. 10.1111/j.1423-0410.1989.tb04981.x.
83. Roubinian, N.H., Plimier, C., Woo, J.P., Lee, C., Bruhn, R., Liu, V.X., Escobar, G.J., Kleinman, S.H., Triulzi, D.J., Murphy, E.L., and Busch, M.P. (2019). Effect of donor, component, and recipient characteristics on hemoglobin increments following red blood cell transfusion. Blood *134*, 1003-1013. 10.1182/blood.2019000773.
84. Donovan, K., Meli, A., Cendali, F., Park, K.C., Cardigan, R., Stanworth, S., McKechnie, S., D'Alessandro, A., Smethurst, P.A., and Swietach, P. (2021). Stored blood has compromised oxygen unloading kinetics that can be normalized with rejuvenation and predicted from corpuscular side-scatter. Haematologica. 10.3324/haematol.2021.279296.
85. Kanias, T., Lanteri, M.C., Page, G.P., Guo, Y., Endres, S.M., Stone, M., Keating, S., Mast, A.E., Cable, R.G., Triulzi, D.J., et al. (2017). Ethnicity, sex, and age are determinants of red blood cell storage and stress hemolysis: results of the REDS-III RBC-Omics study. Blood Adv *1*, 1132-1141. 10.1182/bloodadvances.2017004820.
86. Zwart, A., van Assendelft, O.W., Bull, B.S., England, J.M., Lewis, S.M., and Zijlstra, W.G. (1996). Recommendations for reference method for haemoglobinometry in human blood (ICSH standard 1995) and specifications for international haemiglobinocyanide standard (4th edition). J Clin Pathol *49*, 271-274. 10.1136/jcp.49.4.271.
87. Judkiewicz, L., Bugala, I., and Bartosz, G. (1989). 'Pink test' and osmotic fragility test for the diagnosis of hereditary spherocytosis: another view. Eur J Haematol *42*, 217. 10.1111/j.1600-0609.1989.tb01216.x.
88. Vettore, L., Zanella, A., Molaro, G.L., De Matteis, M.C., Pavesi, M., and Mariani, M. (1984). A new test for the laboratory diagnosis of spherocytosis. Acta Haematol *72*, 258-263. 10.1159/000206398.
89. Nemkov, T., Yoshida, T., Nikulina, M., and D'Alessandro, A. (2022). High-Throughput Metabolomics Platform for the Rapid Data-Driven Development of Novel Additive Solutions for Blood Storage. Frontiers in Physiology *13*. 10.3389/fphys.2022.833242.
90. Thomas, T., Stefanoni, D., Dzieciatkowska, M., Issaian, A., Nemkov, T., Hill, R.C., Francis, R.O., Hudson, K.E., Buehler, P.W., Zimring, J.C., et al. (2020). Evidence for structural protein damage and membrane lipid remodeling in red blood cells from COVID-19 patients. medRxiv. 10.1101/2020.06.29.20142703.
91. Reisz, J.A., Zheng, C., D'Alessandro, A., and Nemkov, T. (2019). Untargeted and Semi-targeted Lipid Analysis of Biological Samples Using Mass Spectrometry-Based Metabolomics. Methods Mol Biol *1978*, 121-135. 10.1007/978-1-4939-9236-2_8.
92. Stephenson, D., Nemkov, T., Qadri, S.M., Sheffield, W.P., and D'Alessandro, A. (2022). Inductively-Coupled Plasma Mass Spectrometry-Novel Insights From an Old Technology Into Stressed Red Blood Cell Physiology. Front Physiol *13*, 828087. 10.3389/fphys.2022.828087.
93. Josephson, C.D., Glynn, S., Mathew, S., Birch, R., Bakkour, S., Baumann Kreuziger, L., Busch, M.P., Chapman, K., Dinardo, C., Hendrickson, J., et al. (2022). The Recipient Epidemiology and Donor Evaluation Study-IV-Pediatric (REDS-IV-P): A research program striving to improve blood donor safety and optimize transfusion outcomes across the lifespan. Transfusion *62*, 982-999. 10.1111/trf.16869.
94. Bakkour, S., Acker, J.P., Chafets, D.M., Inglis, H.C., Norris, P.J., Lee, T.-H., and Busch, M.P. (2016). Manufacturing method affects mitochondrial DNA release and extracellular vesicle composition in stored red blood cells. Vox Sanguinis *111*, 22-32. https://doi.org/10.1111/vox.12390.
95. Nemkov, T., Yoshida, T., Nikulina, M., and D'Alessandro, A. (2022). High-Throughput Metabolomics Platform for the Rapid Data-Driven Development of Novel Additive Solutions for Blood Storage. Front Physiol *13*, 833242. 10.3389/fphys.2022.833242.

96. Nemkov, T., Reisz, J.A., Gehrke, S., Hansen, K.C., and D'Alessandro, A. (2019). High-Throughput Metabolomics: Isocratic and Gradient Mass Spectrometry-Based Methods. Methods Mol Biol *1978*, 13-26. 10.1007/978-1-4939-9236-2_2.
97. Stefanoni, D., Shin, H.K.H., Baek, J.H., Champagne, D.P., Nemkov, T., Thomas, T., Francis, R.O., Zimring, J.C., Yoshida, T., Reisz, J.A., et al. (2020). Red blood cell metabolism in Rhesus macaques and humans: comparative biology of blood storage. Haematologica *105*, 2174-2186. 10.3324/haematol.2019.229930.
98. Nemkov, T., Hansen, K.C., and D'Alessandro, A. (2017). A three-minute method for high-throughput quantitative metabolomics and quantitative tracing experiments of central carbon and nitrogen pathways. Rapid Commun Mass Spectrom *31*, 663-673. 10.1002/rcm.7834.
99. Thomas, T., Stefanoni, D., Dzieciatkowska, M., Issaian, A., Nemkov, T., Hill, R.C., Francis, R.O., Hudson, K.E., Buehler, P.W., Zimring, J.C., et al. (2020). Evidence of Structural Protein Damage and Membrane Lipid Remodeling in Red Blood Cells from COVID-19 Patients. J Proteome Res *19*, 4455-4469. 10.1021/acs.jproteome.0c00606.
100. Salyer, S.W. (2007). Chapter 11 - Hematologic Emergencies. In Essential Emergency Medicine, S.W. Salyer, ed. (W.B. Saunders), pp. 555-574. https://doi.org/10.1016/B978-141602971-7.10011-X.
101. Moore, A., Busch, M.P., Dziewulska, K., Francis, R.O., Hod, E.A., Zimring, J.C., D'Alessandro, A., and Page, G.P. (2022). Genome-wide metabolite quantitative trait loci analysis (mQTL) in red blood cells from volunteer blood donors. J Biol Chem *298*, 102706. 10.1016/j.jbc.2022.102706.
102. Wei, R., Wang, J., Su, M., Jia, E., Chen, S., Chen, T., and Ni, Y. (2018). Missing Value Imputation Approach for Mass Spectrometry-based Metabolomics Data. Scientific Reports *8*, 663. 10.1038/s41598-017-19120-0.
103. Ongen, H., Buil, A., Brown, A.A., Dermitzakis, E.T., and Delaneau, O. (2016). Fast and efficient QTL mapper for thousands of molecular phenotypes. Bioinformatics *32*, 1479-1485. 10.1093/bioinformatics/btv722.
104. Guo, Y., Busch, M.P., Seielstad, M., Endres-Dighe, S., Westhoff, C.M., Keating, B., Hoppe, C., Bordbar, A., Custer, B., Butterworth, A.S., et al. (2019). Development and evaluation of a transfusion medicine genome wide genotyping array. Transfusion *59*, 101-111. 10.1111/trf.15012.
105. Delaneau, O., Coulonges, C., and Zagury, J.-F. (2008). Shape-IT: new rapid and accurate algorithm for haplotype inference. BMC Bioinformatics *9*, 540. 10.1186/1471-2105-9-540.
106. Howie, B., Marchini, J., and Stephens, M. (2011). Genotype Imputation with Thousands of Genomes. G3 Genes|Genomes|Genetics *1*, 457-470. 10.1534/g3.111.001198.
107. Zheng, X., Levine, D., Shen, J., Gogarten, S.M., Laurie, C., and Weir, B.S. (2012). A high-performance computing toolset for relatedness and principal component analysis of SNP data. Bioinformatics *28*, 3326-3328. 10.1093/bioinformatics/bts606.
108. Aulchenko, Y.S., Struchalin, M.V., and van Duijn, C.M. (2010). ProbABEL package for genome-wide association analysis of imputed data. BMC Bioinformatics *11*, 134. 10.1186/1471-2105-11-134.
109. Perry, J.A., Gaynor, B.J., Mitchell, B.D., and O'Connell, J.R. (2021). An Omics Analysis Search and Information System (OASIS) for Enabling Biological Discovery in the Old Order Amish. bioRxiv, 2021.2005.2002.442370. 10.1101/2021.05.02.442370.
110. Howie, H.L., Hay, A.M., de Wolski, K., Waterman, H., Lebedev, J., Fu, X., Culp-Hill, R., D'Alessandro, A., Gorham, J.D., Ranson, M.S., et al. (2019). Differences in Steap3 expression are a mechanism of genetic variation of RBC storage and oxidative damage in mice. Blood Adv *3*, 2272-2285. 10.1182/bloodadvances.2019000605.
111. Churchill, G.A., Gatti, D.M., Munger, S.C., and Svenson, K.L. (2012). The Diversity Outbred mouse population. Mamm Genome *23*, 713-718. 10.1007/s00335-012-9414-2.
112. Morgan, A.P., and Welsh, C.E. (2015). Informatics resources for the Collaborative Cross and related mouse populations. Mamm Genome *26*, 521-539. 10.1007/s00335-015-9581-z.
113. Broman, K.W., Gatti, D.M., Simecek, P., Furlotte, N.A., Prins, P., Sen, Ś., Yandell, B.S., and Churchill, G.A. (2019). R/qtl2: Software for Mapping Quantitative Trait Loci with High-Dimensional Data and Multiparent Populations. Genetics *211*, 495-502. 10.1534/genetics.118.301595.

114. Keele, G.R. (2023). Which mouse multiparental population is right for your study? The Collaborative Cross inbred strains, their F1 hybrids, or the Diversity Outbred population. G3 (Bethesda) *13*. 10.1093/g3journal/jkad027.
115. Vincent, M., Gerdes Gyuricza, I., Keele, G.R., Gatti, D.M., Keller, M.P., Broman, K.W., and Churchill, G.A. (2022). QTLViewer: an interactive webtool for genetic analysis in the Collaborative Cross and Diversity Outbred mouse populations. G3 (Bethesda) *12*. 10.1093/g3journal/jkac146.
116. https://biolincc.nhlbi.nih.gov/studies/reds_iii/.
117. Karafin, M.S., Bruhn, R., Westlake, M., Sullivan, M.T., Bialkowski, W., Edgren, G., Roubinian, N.H., Hauser, R.G., Kor, D.J., Fleischmann, D., et al. (2017). Demographic and epidemiologic characterization of transfusion recipients from four US regions: evidence from the REDS-III recipient database. Transfusion *57*, 2903-2913. 10.1111/trf.14370.
118. Endres-Dighe, S.M., Guo, Y., Kanias, T., Lanteri, M., Stone, M., Spencer, B., Cable, R.G., Kiss, J.E., Kleinman, S., Gladwin, M.T., et al. (2019). Blood, sweat, and tears: Red Blood Cell-Omics study objectives, design, and recruitment activities. Transfusion *59*, 46-56. 10.1111/trf.14971.
119. Pang, Z., Chong, J., Zhou, G., de Lima Morais, D.A., Chang, L., Barrette, M., Gauthier, C., Jacques, P.-É., Li, S., and Xia, J. (2021). MetaboAnalyst 5.0: narrowing the gap between raw spectra and functional insights. Nucleic Acids Research *49*, W388-W396. 10.1093/nar/gkab382.

FIGURES

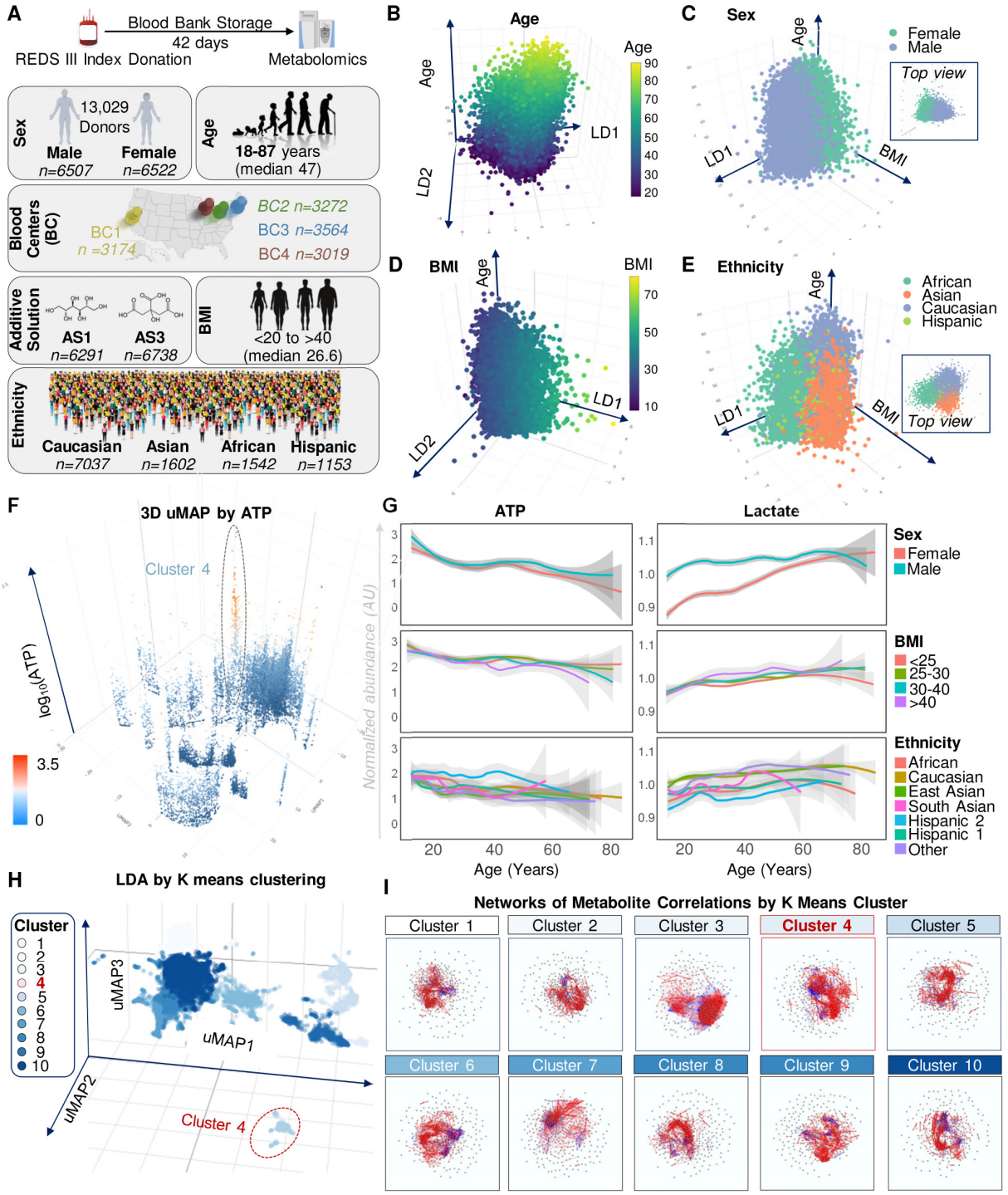

Figure 1 – Metabolomics of 13,029 end of storage packed RBCs from the REDS RBC Omics Index cohort Leukocyte-filtered red blood cells (RBCs) were donated by 13,029 volunteers across four different blood centers in the United States and stored for 42 days (end of the shelf-life) prior to testing via high-throughput metabolomics. In **A,** an overview of the study design and donor demographics (sex, age, ethnicity), blood centers (BC) and additive solutions (AS). In **B-E**, linear discriminant analysis (LDA) of metabolomics data in this cohort as a function of donor age, sex, body mass index (BMI) and ethnicity, respectively. In **F**, Uniform Manifold Approximation and Projection (uMAP) for

dimension reduction of metabolomics data identifies a cluster of donors with elevated ATP (-log10 of arbitrary units for ATP on the z axis). In **C,** linear discriminant analysis color-coded as a function of K mean clustering analysis. In **D**, network view of metabolite-metabolite correlations (Spearman) as a function of the 10 K means clusters. Each metabolite is a node and a red and blue edge indicates positive or negative correlations higher than 0.5 in module. In **E**, Uniform Manifold Approximation and Projection (uMAP) of the metabolomics data from all 13,029 index donors color-coded by ATP levels. In **F**, heat map of the top 50 significant metabolites that discriminate the donors with the lowest and highest ATP levels (5th and 95th percentiles; n=700). In **G,** donor age, sex and ethnicity, but not BMI, significantly impact the levels of ATP and lactate in end of storage RBCs (x axis is donor age for all the line plots). In **H**, K means clustering analysis highlights 10 clusters, and the metabolic profiles of donors in cluster 4 separate them from the rest of the samples. In **I**, metabolite-metabolite interactions are independently shown for all donors in each cluster (red vs blue indicates correlations with positive or negative modules higher than 0.75, respectively).

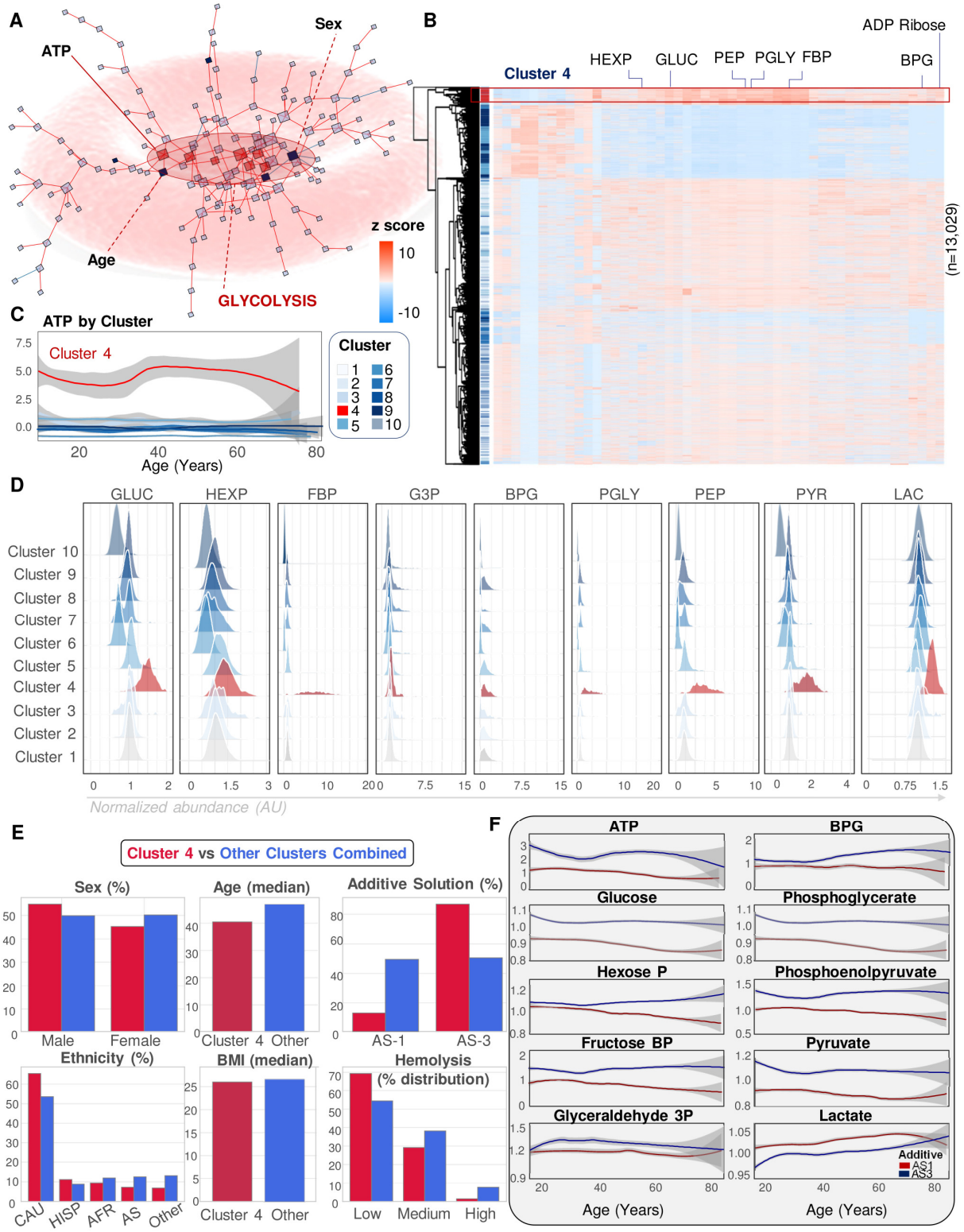

Figure 2 – Cluster 4 is characterized by elevated glycolytic metabolites, high ATP and low hypoxanthine. In **A**, network view of the most significant metabolite-metabolite interactions across the whole dataset confirms the centrality of glycolytic metabolism in stored RBCs. In **B**, hierarchical clustering analysis (top 50 metabolites by ANOVA) of index donors based on grouping derived by K means clustering for latent variables (cluster 4 in red). Glycolytic metabolites are abbreviated, including glucose (GLUC), hexose phosphate (HEXP), fructose bisphosphate (FBP), glyceraldehyde 3-phosphate (G3P), 2,3-bisphosphoglycerate (BPG), phosphoglycerate (PGLY), phosphoenolpyruvate (PEP), pyruvate (PYR), lactate (LAC), all highest in donors in cluster 4 (red). In **D**, ridge plots for all glycolytic intermediates show

increases of glucose and all glycolytic metabolites in donors from cluster 4 (red). In **E**, donor demographics and hemolysis for cluster 4 (red) vs all the other clusters combined (blue). In **F**, glycolysis by storage additive (AS1 in red, AS3 in blue).

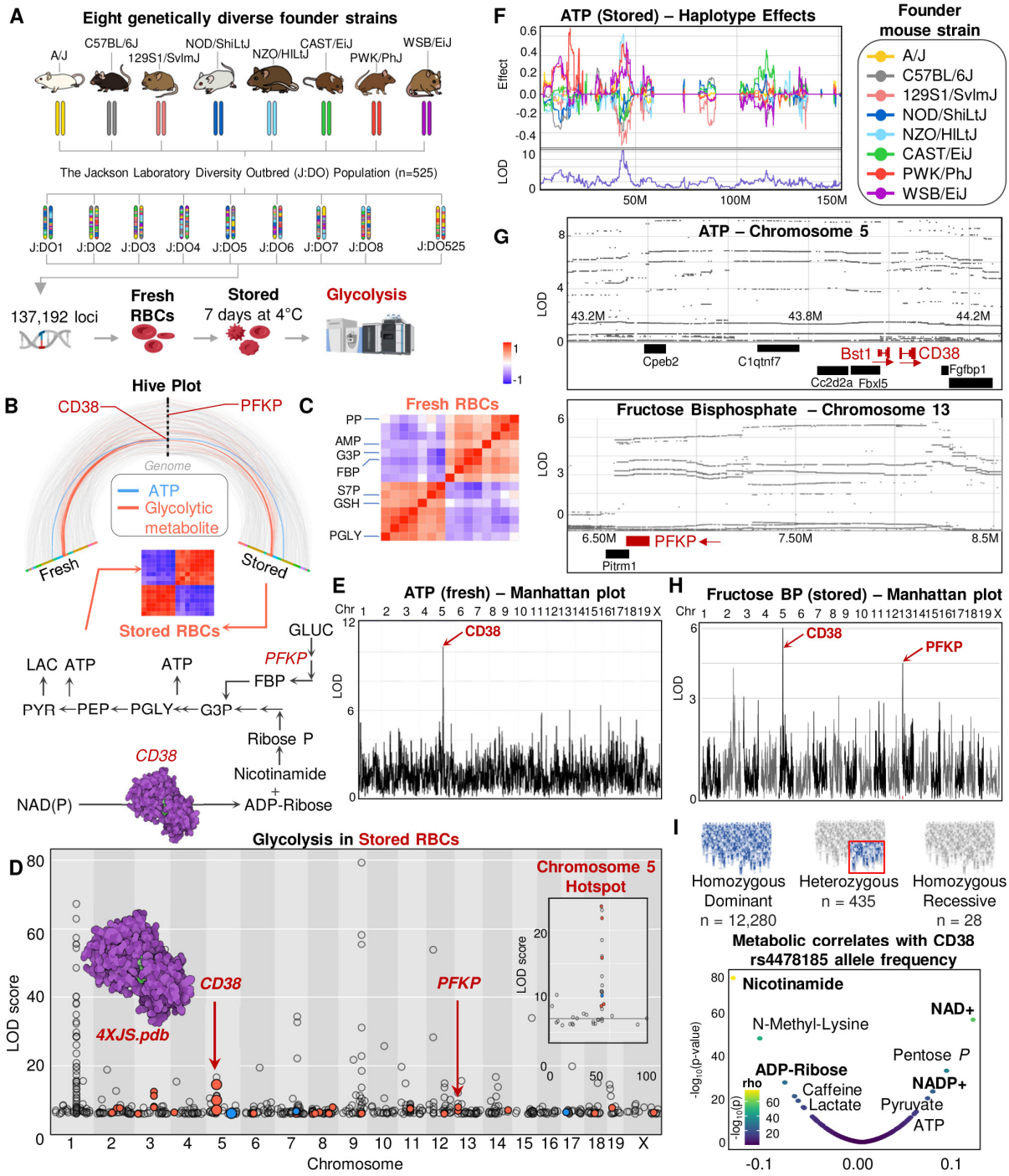

Figure 3 – Association between glycolysis and CD38 polymorphisms in fresh and stored murine RBCs from the Diversity Outbred population. Metabolomics analysis was performed in fresh and stored RBCs from 525 mice derived from extensive cross-breeding (>46 generations) of 8 genetically distinct founder strains (Jackson Laboratory's Diversity Outbred – J:DO – **A**). A hot spot of mQTL were identified on chromosomes 5 and 13 – hive plot (n=525 - **B**). Heat maps of metabolic correlates to the locus on chromosome 5 in fresh (**C**) and stored RBCs (**B**). Manhattan plot for merged glycolytic metabolites, with highlighted a hotspot region on chromosome 5 (n = 525 - **D**), which codes for CD38 and associates with all glycolytic and pentose phosphate pathway (PPP) metabolites in stored murine RBCs. In **E**, CD38/BST1

was associated with ATP levels in fresh and stored murine RBCs (n=350 - Manhattan plot, Best Linear Unbiased Predictors and Locus Zoom in **E-F-G,** respectively). Less significant, but still above FDR-corrected threshold, both CD38 and PFKP were found to associate with fructose bisphosphate (FBP) levels in stored RBCs (locus Zoom in **G,** and Manhattan plot in **H**). In **I,** the SNP rs4478185 was identified as the top CD38 SNPs associated with glycolysis and PPP metabolites in human RBCs from the REDS RBC Omics Index cohort confirming observations in mice.

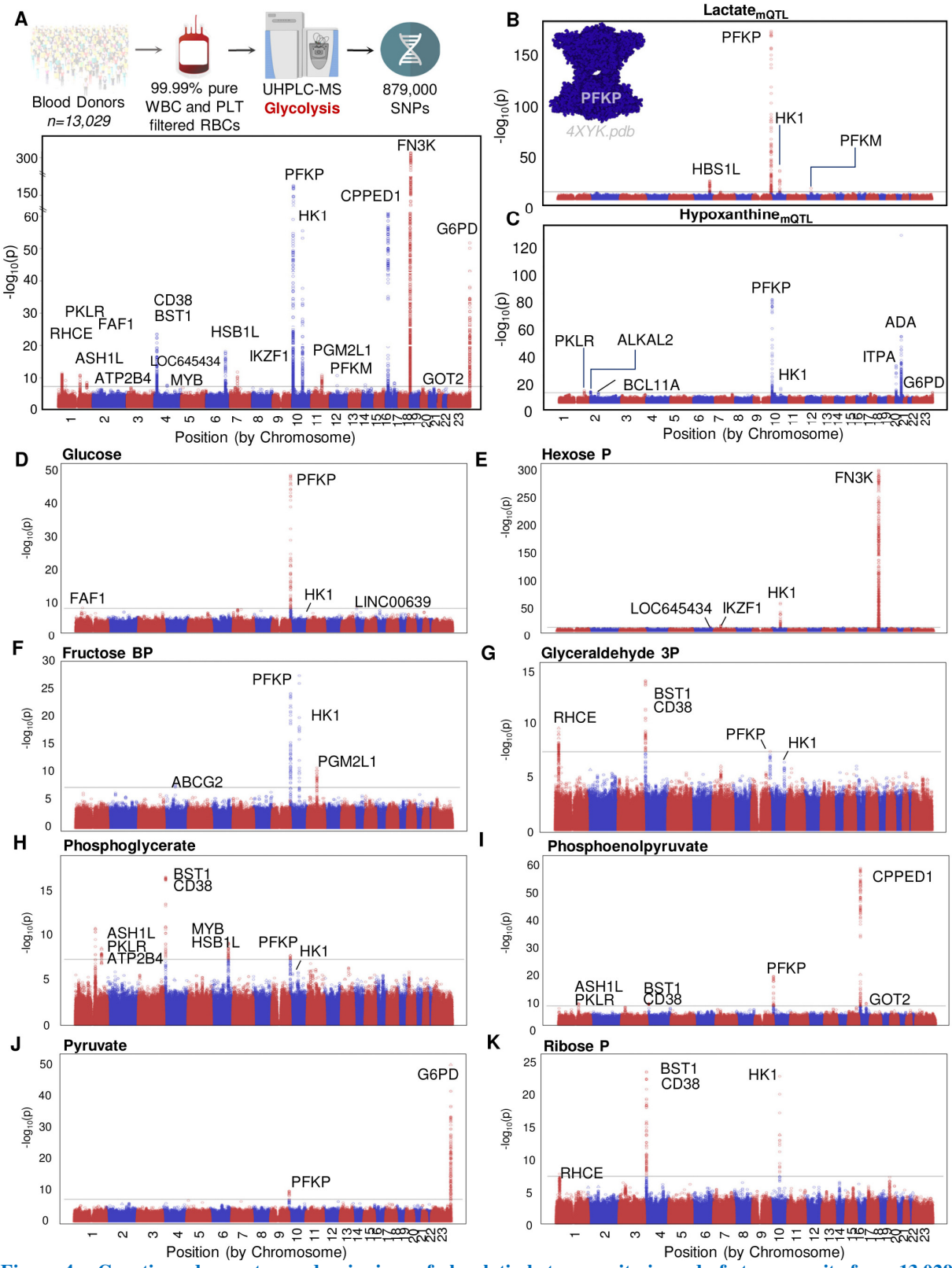

Figure 4 – Genetic and ancestry underpinnings of glycolytic heterogeneity in end of storage units from 13,029 REDS RBC Omics Index donors. Along with metabolomics analyses, as part of the REDS RBC Omics study we tested donors for ~879,000 single nucleotide polymorphisms (SNPs – **A**). Official gene symbols are used to abbreviate all FDR-corrected significant hits (corrected p-value threshold of $5x10^{-8}$) in the summary Manhattan plot of metabolite Quantitative Trait Loci (mQTL) for all glycolytic metabolites merged (**A**), or just for lactate (**B**) and hypoxanthine (**C**). Independent

Manhattan plots are shown for all glycolytic metabolites and ribose phosphate (**D-K**). Locus zoom plots in **Supplementary Figure 2-4**. Abbreviations: P: phosphate; BP: bisphosphate; Gene names are listed with their official gene symbols. *Abbreviations:* ASH1L: Histone-lysine N-methyltransferase ASH1L; BST1: ADP-ribosyl cyclase 2; CD38: ADP-ribosyl cyclase 1; CPPED1: Ser/Thr-protein phosphatase CPPED1; FAF1: FAS-associated factor 1; FN3K: Fructosamine-3-kinase; G6PD: Glucose-6-phosphate 1-dehydrogenase; GOT2: Aspartate aminotransferase; HBS1L: HBS1-like protein; HK1: Hexokinase-1; ITPA: Inosine Triphosphate Pyrophosphatase; MYB: Transcriptional activator Myb; PFKM: ATP-dependent 6-phosphofructokinase, muscle type; PFKP: ATP-dependent 6-phosphofructokinase, platelet type; PKLR: Pyruvate kinase; RHCE: Blood group Rh(CE).

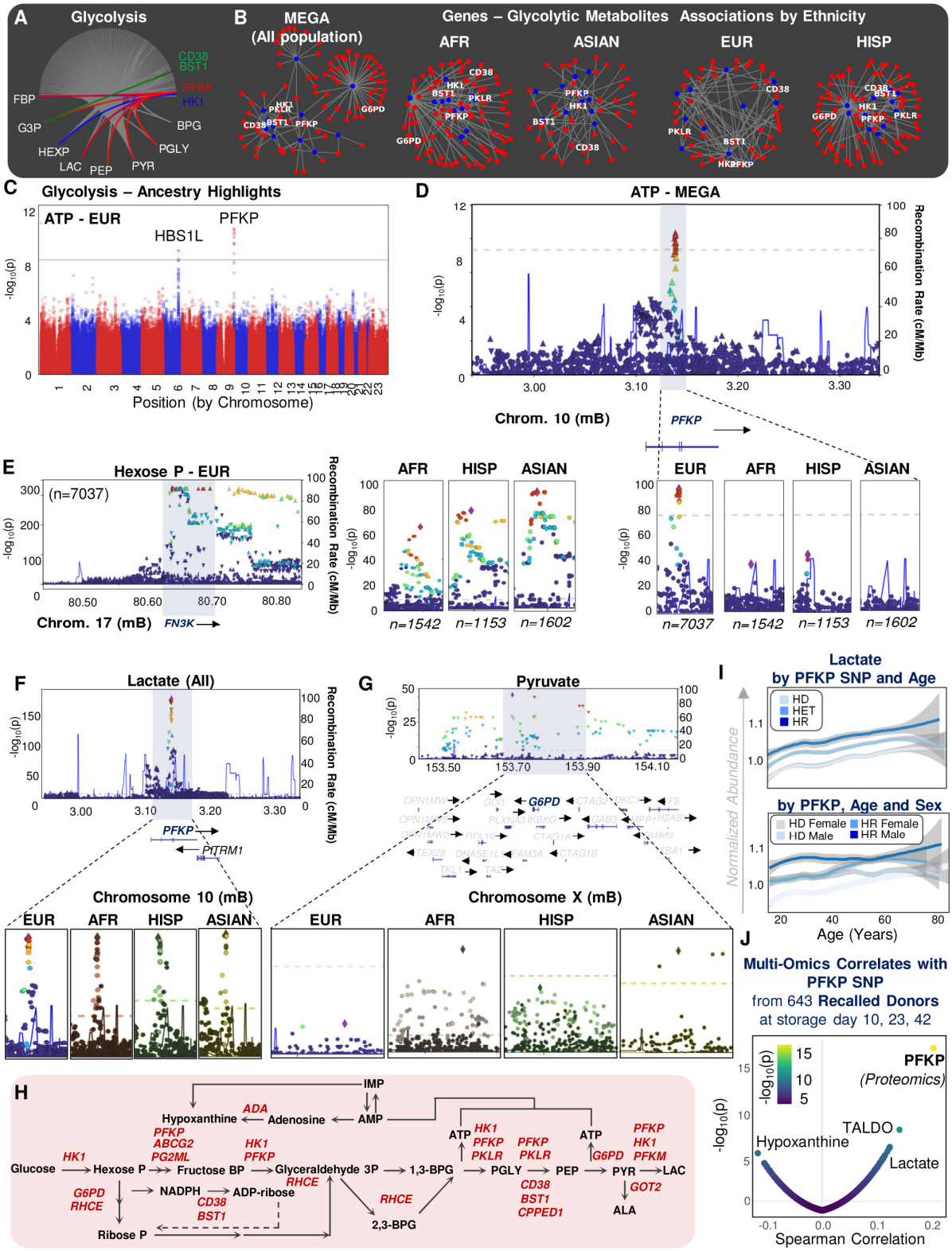

Figure 5 – mQTL analyses by ancestry In **A**, the circos plot summarizes the main gene-glycolytic metabolite associations (official gene symbols). In **B**, network view of gene-glycolytic metabolite interactions broken down by ethnicity (MEGA: All population; AFR: African American; Eur: European; HISP: Hispanic – detailed results of the ancestry-based analysis are provided in **Supplementary Table 1**). In **C-D**, Manhattan plot and locus zoom plot for ATP by ancestry, with a locus zoom highlight for the region coding for PFKP on chromosome 10. In **E-G**, locus zoom plots

for lactate, pyruvate and hexose phosphate on regions coding for PFKP, G6PD and FN3K, resepctively. Specifically, the mQTL breakdown by ancestry for PKFP SNPs on chromosome 10 was observed across all populations for lactate (**F**), but glucose 6-phosphate dehydrogenase (G6PD African variant V68M) SNPs on chromosome X exclusively observed in donors of African descent, followed by Asian descent, but not in donors of European or Hispanic ancestry (**G**). In **H**, a summary overview of the gene-metabolite associations identified by the mQTL analysis (official gene symbols are listed in red on top of the reaction generating the metabolite they have been linked to in our analysis on the whole population). In **I**, combined effects of PFKP SNP with donor age (top) and sex (bottom) for lactate. HD: homozygous dominant (i.e., 0 alleles of rs2388595); HET: heterozygous (1 allele); HR: homozygous recessive (2 alleles). In **J**, multi-omics analyses of recalled donor units (n=643, storage day 10, 23, 42) confirmed a strong positive correlation between phosphofructokinase platelet isoform - PFKP SNP rs2388595 alleles and PFKP levels by proteomics, and positive and negative associations with lactate and hypoxanthine.

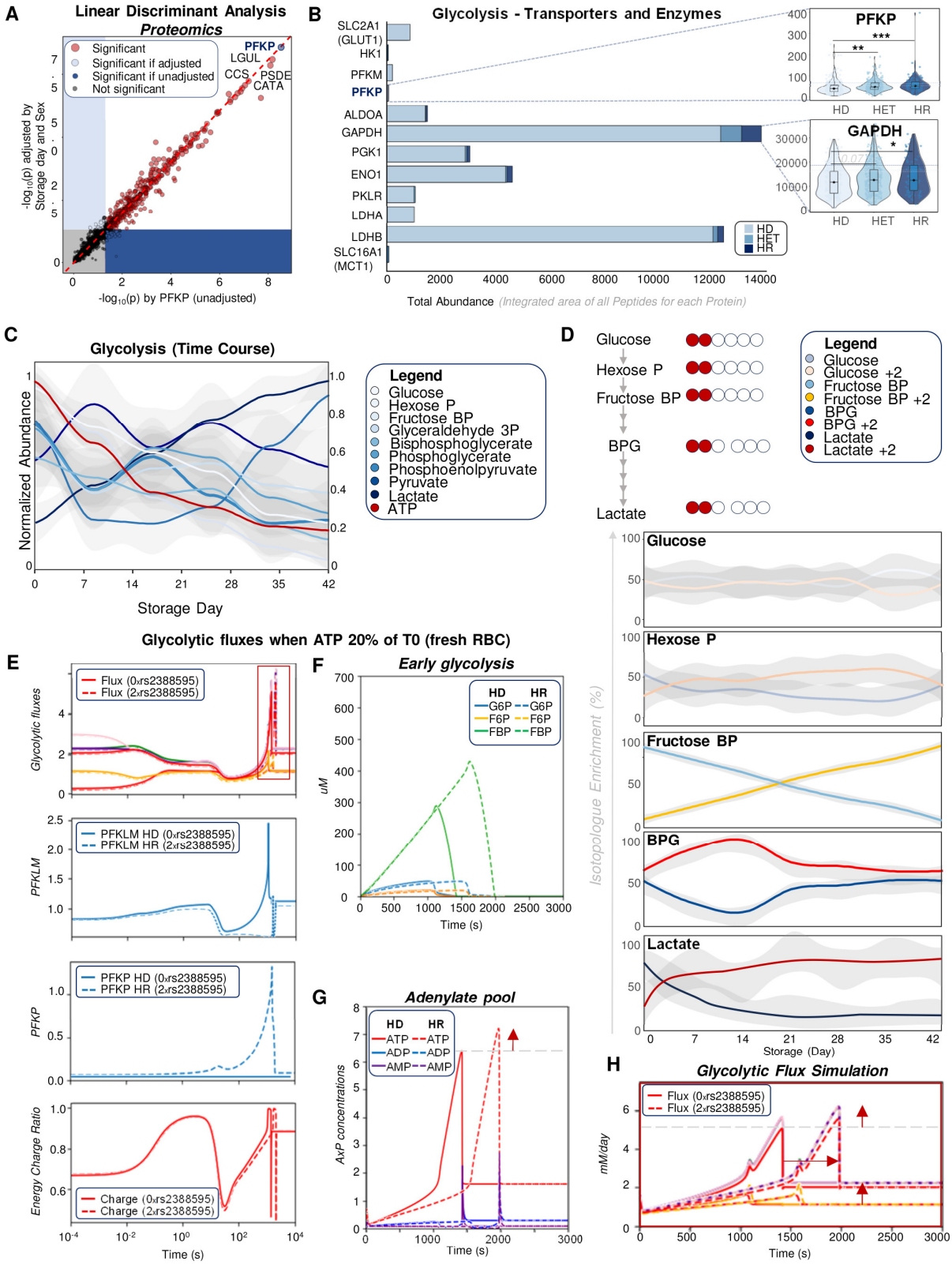

Figure 6 – Metabolic reconstruction of glycolytic fluxes as a function of PFKP genotypes, proteomics and metabolomics data. Linear discriminant analysis (LDA) of proteomics data – either unadjusted (x axis) or adjusted by storage age and sex (y axis) confirms an association between allele copy number for PFKP SNP rs2388595 and protein levels of phosphofructokinase P (PFKP) (**A**). In **B**, total abundance (integrated peak area, arbitrary units) for all

transporters and enzymes glycolytic proteins (official gene symbols) in RBCs from the REDS RBC Omics recalled donors (n=643; storage day 42). No significant changes in the levels of any of these proteins were observed over storage (day 10, 23 and 42 – **Supplementary Figure 5.F**). In **C**, weekly measurements of glycolytic metabolites in fresh units of packed RBCs through the end of storage (day 42 – median ± quartiles are shown; n = 6). In **D**, storage experiments in C were repeated by adding 1,2-$^{13}C_2$-glucose and tracing ^{13}C unlabeled vs labeled isotopologues as percentage of the total levels of each metabolite. In **E**, glycolytic flux estimates from reconstruction models of RBC metabolism over time (x axis), with relative contribution of phosphofructokinase (PFK) isoform LM and P in donors carrying 0 (continuous lines) or 2 alleles (dotted lines) of the rs2388595 SNP, based on the PFKP abundance estimates derived from the proteomics data. Early glycolysis (glucose 6-phosphate – G6P; fructose 6-phosphate – F6P; fructose 1,6-bisphosphate – FBP - **F**) and total adenylate pool (AxP – AMP + ADP + ATP - **G**) and zoom in on glycolytic fluxes (**H**) as a function of rs2388595 alleles, respectively.

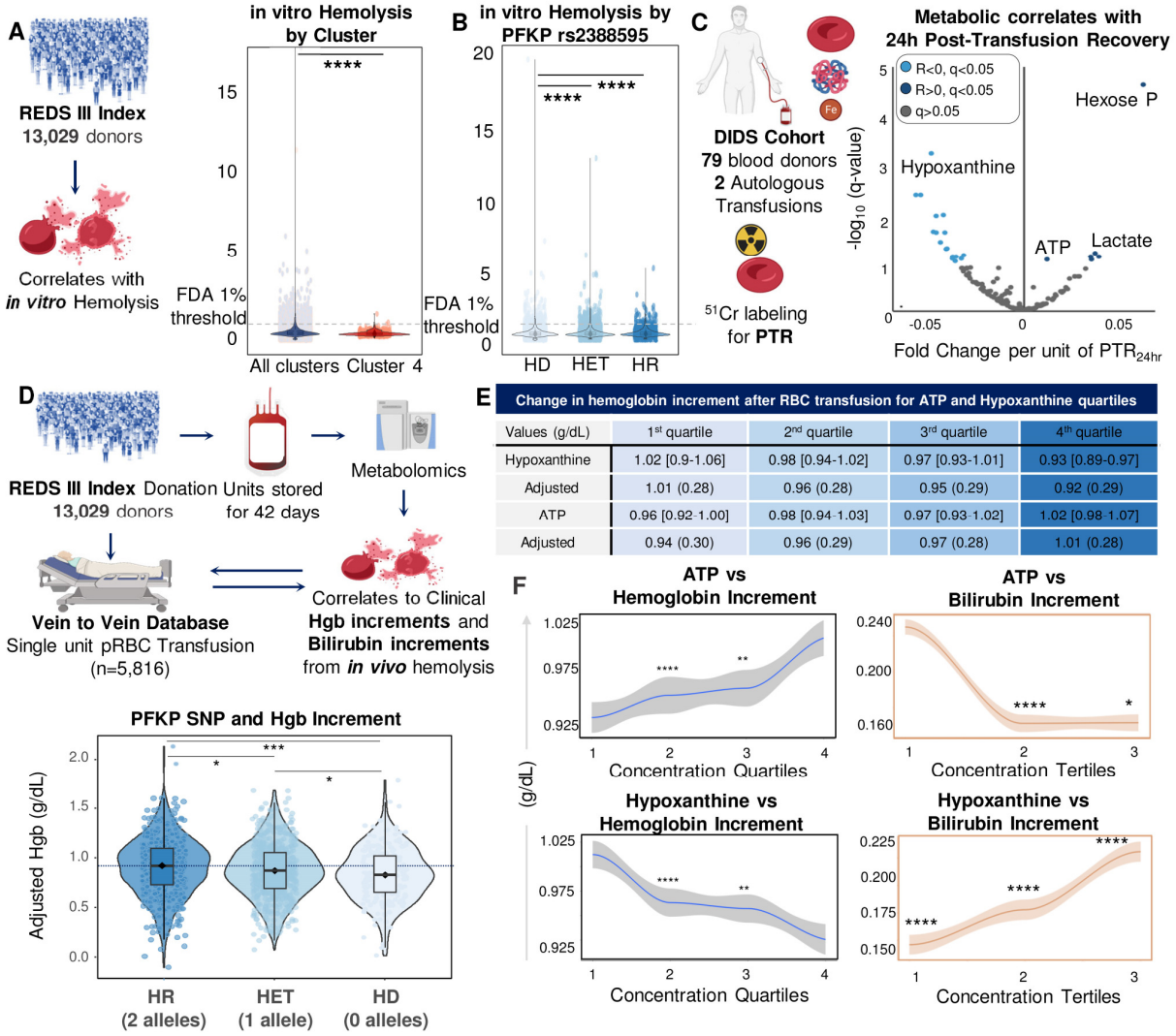

Change in hemoglobin increment after RBC transfusion for ATP and Hypoxanthine quartiles

Values (g/dL)	1st quartile	2nd quartile	3rd quartile	4th quartile
Hypoxanthine	1.02 [0.9-1.06]	0.98 [0.94-1.02]	0.97 [0.93-1.01]	0.93 [0.89-0.97]
Adjusted	1.01 (0.28)	0.96 (0.28)	0.95 (0.29)	0.92 (0.29)
ATP	0.96 [0.92-1.00]	0.98 [0.94-1.03]	0.97 [0.93-1.02]	1.02 [0.98-1.07]
Adjusted	0.94 (0.30)	0.96 (0.29)	0.97 (0.28)	1.01 (0.28)

Figure 7 – Positive and negative association of glycolysis/ATP and hypoxanthine to in vitro and in vivo hemolysis in healthy and critically ill individuals receiving autologous and non-autologous transfusion, respectively. End of storage spontaneous hemolysis - one of the two FDA gold standards for the quality of stored pRBC products - was measured in all 13,029 units. Lactate levels at storage day 42 were the top predictor of spontaneous hemolysis (**A**). Units from donors in cluster 4 (**A**) or donors carrying two alleles of the PFKP SNP 2388595 (**B**) showed significantly lower levels of end of storage in bag hemolysis than units from donors in other clusters or not carrying any allele with that SNP. In a separate cohort of 79 healthy volunteer donations and autologous transfusion events, glycolytic metabolites and ATP levels were positively associated to, and hypoxanthine negatively associated to measurements of post-transfusion recovery with ^{51}Cr in healthy volunteers – the other FDA gold standard for monitoring the quality of stored RBCs (**C**). By accessing the "vein-to-vein" database of the REDS RBC Omics program, we could link adjusted hemoglobin increments in clinical recipients of irradiated single pRBC unit transfusions to blood donor PFKP status for rs2388595; abbreviations:

homozygous dominant = HD, i.e., carrying 0 alleles of the SNP n=521; heterozygous = HET 1 allele, n=576; homozygous recessive = HR, 2 alleles, n=204 (**D**). Similarly, we linked end of storage ATP and hypoxanthine levels to hemoglobin increments (n=5,816 records available in the database) and bilirubin increments (n=914) upon heterologous transfusion of products from the same donors to critically ill recipients requiring transfusion (**E-F**).